Geological Quarterly, 2025, 69, 42
DOI: https://doi.org/10.7306/gq.1815

Sinuous ridges in the Polesie region (SE Poland) as inverted fluvial channels: morphology, structure and genesis

Mirosław KRAWCZYK[1, *] and Magdalena KUCHARSKA[1]

[1] Polish Geological Institute – National Research Institute, Rakowiecka 4, 00-975 Warszawa, Poland; ORCID 0000-0001-9891-7455 [M.Kr.], 0000-0003-0136-6138 [M.K.]

Krawczyk, M., Kucharska, M., 2025. Sinuous ridges in the Polesie region (SE Poland) as inverted fluvial channels: morphology, structure and genesis. Geological Quarterly, 69, 42; https://doi.org/10.7306/gq.1815

Associate Editor: Wojciech Granoszewski

We describe unique forms of sinuous ridges found only in Polesie, Poland, described from elesewhere in the world as palaeochannels and inverted fluvial channels. Sinuous ridges documented in Polesia represent two genetic types: glacial forms and inverted fluvial channels. The examples described of inverted fluvial channels are the only ones of this type documented in Poland. They formed at the transition between the Vistulian and Holocene, as a result of deposition of fine-grained sediments in fossil subglacial troughs. As a result of climatic changes and warming as the Vistulian gave way to the Holocene, the ice sheet covering the floodplains in the area thawed, and positive forms were formed from the deposits that had accumulated in channels in the ice. An important factor intensifying the process of inverted fluvial channel formation in Polesie was the mechanical properties of the rocks. Under specific climatic and geological conditions, with a high water content, the carbonate rocks building the sub-Quaternary substrate were subject to swelling. This resulted in the upward pushing of deposits accumulated in the troughs and the eventual formation of sinuous ridges. Our results reveal new mechanisms and considers new factors in the formation of sinuous ridges of inverted fluvial channel type, which can be applied at a planetary scale.

Key words: sinuous ridges, inverted fluvial channels, Polesie Plain, Pleistocene changes.

INTRODUCTION

During the preparation of the Detailed Geological Map of Poland (abbreviated as SMGP below, from the Szczegółowa Mapa Geologiczna Polski), on the Ostrów Lubelski (Krawczyk, 2023a, b), Orzechów Nowy (Krawczyk, 2023a, b), Łęczna (Krawczyk and Kucharska, 2023a, b) and Sawin (Kucharska, 2025a, b) sheets, very unusual landforms were observed in the study area. These were characteristic sinuous ridges, oriented in N–S, NW–SE and NE–SW directions. The Digital Terrain Model (DTM) image showed that many of these isolated forms are arranged in chains up to several tens of kilometres long (Fig. 1). Initial palaeogeographic analysis and DTM suggested that many of them may be inverted channels (e.g., LeConte, 1880; Pain and Ollier, 1995; Pain et al., 2007; Williams et al., 2007; Zaki et al., 2021) as opposed to glacial fissures, which are very similar in appearance.

Ridge forms in Polesie had already been observed during earlier research, especially during preparation of the SMGP in 1997–2017 (Fig. 1). However, these forms had not been fully studied. The authors of individual SMGP map sheets focused on individual forms, most often found within a single SMGP sheet, ignoring their broader palaeogeographic context. Their geological structure, age and origin were interpreted in various ways. They were most often considered as postglacial forms from the Middle Polish Glaciation or as fluvioperiglacial deposits from the Vistulian Glaciation, often with different origins or ages within a single study (Liszkowski, 1979a, b; Stochlak, 1979a, b; Buraczyński and Wojtanowicz, 1981a, b, 1982a, b, 1987a, b; Harasimiuk et al., 2017). Many of the smaller or less distinct forms were omitted from the maps (Fig. 1).

In Poland, only two authors: Maruszczak (1974a, b) and Liszkowski (1979a, b), attempted to explain the age and origin of these unusual sinuous ridges found in Polesie. Maruszczak (1974a, b) was the first to draw attention to them. He described them as a 'peculiar variety of kem-type forms' and linked their origin to the movement of water over the stagnant ice sheet during the glaciation of the Oder River. Liszkowski (1979a, b) studying their sedimentary characteristics and the directions of sediment transport, described the sinuous ridges as fluvioperiglacial deposits from the Odranian glaciation. According to Liszkowski (1979a, b), rivers flowed from the south, over the surface of the ice sheet, carving out their channels, in which sediments were deposited. As a result of the melting of the ice, positive landforms were created, which Liszkowski (1979a, b) described as 'pseudokemic ridges'. These two authors never returned to this issue in their later studies.

* Corresponding author, e-mail: miroslaw.krawczyk@pgi.gov.pl

Received: Received: June 17, 2025; accepted: October 13, 2025; first published online: November 28, 2025

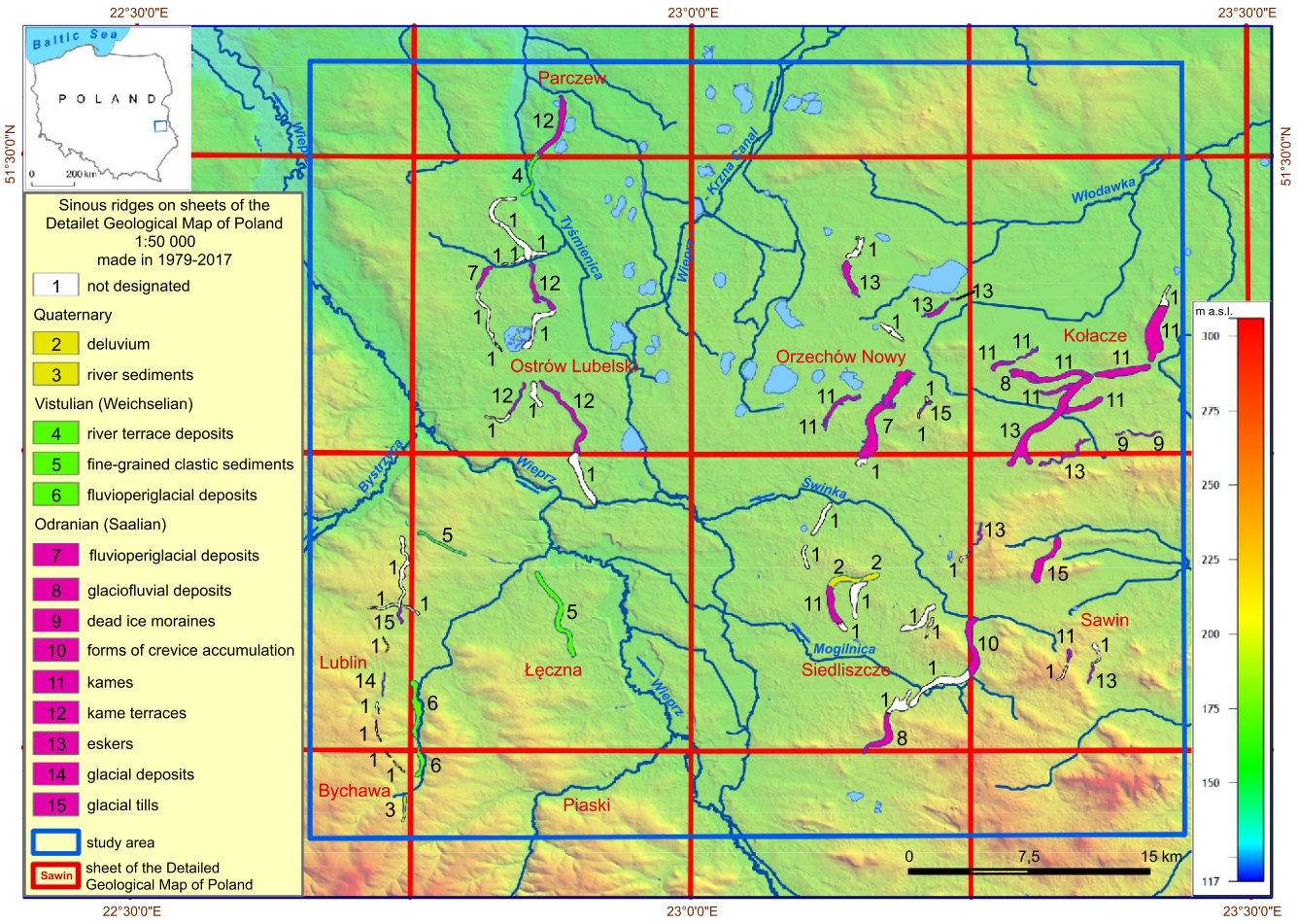

Fig. 1. Distribution of sinuous ridges in Polesie, taking into account the genesis shown on SMGP maps made in 1979–2017

Forms of sinuous ridges interpreted as inverted fluvial channels and inverted channels have been known and documented since the 19th century. Whitney (1865) described 'old river beds' in California, which now form hilltops. His research on inverted channels was continued by LeConte (1880, 1886).

Today, there is a wealth of literature describing inverted channels (e.g., Maizels, 1990; Biek et al., 2000; Mohrig et al., 2000; Aref, 2003; Schuster et al., 2005; Hou et al., 2007; McQueen et al., 2007; Williams et al., 2007, 2021; Ollier and Scheth, 2008; Beresford-Jones et al., 2009; Bristow et al., 2009; Cuevas Martínez et al., 2010; Smith et al., 2010; Cas et al., 2011; Lucchitta, 2011; Foix et al., 2012; Girard et al., 2012; Bell and Williamson, 2013; Butt and Bristow, 2013; Doctor et al., 2014; Morgan et al., 2014; Keller and Morgan, 2016; Matter et al., 2016; Zaki and Giegengack, 2016; Giegengack and Zaki, 2017; Wang et al., 2017; Bussert et al., 2018; Foix et al., 2018; Wang and Bhattacharya, 2018; Zaki et al., 2018, 2020; Ghosh and Guchhait, 2019).

Recent studies of the Mars surface have revealed the existence of sinuous ridges that closely resemble those documented on Earth. Currently, a great deal of research on sinuous ridges, and inverted channels in particular, is being conducted on Earth in order to draw conclusions about the origin of the forms discovered on Mars (e.g., Williams and Edgett, 2005; Pain et al, 2007; Williams et al., 2007, 2009, 2011, 2018; Clarke and Stoker, 2011; Morgan et al., 2014; Matsubara et al., 2015; Jacobsen and Burr, 2017; Hayden et al., 2019; Zaki et al., 2021, 2022). Therefore, the genesis of these types of forms has once again become the subject of wider scientific interest.

The main factors contributing to the formation of inverted channels are filling of the channel with sediment, its cementation, and subsequent exhumation of channel sediments as a positive form (e.g., Pain et al., 2007; Williams et al., 2009; Hayden et al., 2019; Zaki et al., 2021). Channel filling usually occurs during fluvial sedimentation (e.g., Schuster et al., 2005; Williams et al., 2007; Zaki et al., 2018, 2020, 2021), but it can also occur as a result of channel filling with volcanic lava (Sias, 2002; Cuevas Martínez et al., 2010; Bell and Williamson, 2013; Zaki et al., 2021). Cementation occurs as a result of chemical reactions, including cementation by $CaCO_3$, SiO_2, and Fe compounds (e.g., Aref, 2003; Worden and Burley, 2003; Williams et al., 2007, 2009). Cementation may also occur as a result of burial of sediments and their lithification deep within the Earth's crust (e.g., Williams et al., 2007, 2011). Another process of inverted channel formation is the creation of an erosion-resistant armour on the surface of the sediment filling the channel, most commonly from coarse-grained sediments (e.g., Pain and Ollier, 1995; Marchetti et al., 2005; Lucchitta, 2011). Palaeochannels have recently been documented on the Atacama Desert in Chile, where palaeochannel deposits were filled with evaporites (Williams et al., 2021).

The exhumation of deposits filling the palaeochannel may result from water erosion (e.g., Maizels, 1990; Williams et al., 2007, 2011, 2021; Zaki et al., 2018), aeolian erosion (e.g., Bristow et al., 2009; Zaki et al, 2018), tectonic exhumation (e.g., Hill et al., 2003; Foix et al., 2012, 2018) and degradation of the channel surroundings, such as compaction or burning of organic sediments such as peats (Gumbricht et al., 2004; Smith et al., 2010). For inverted channels to form, many of these factors must coexist.

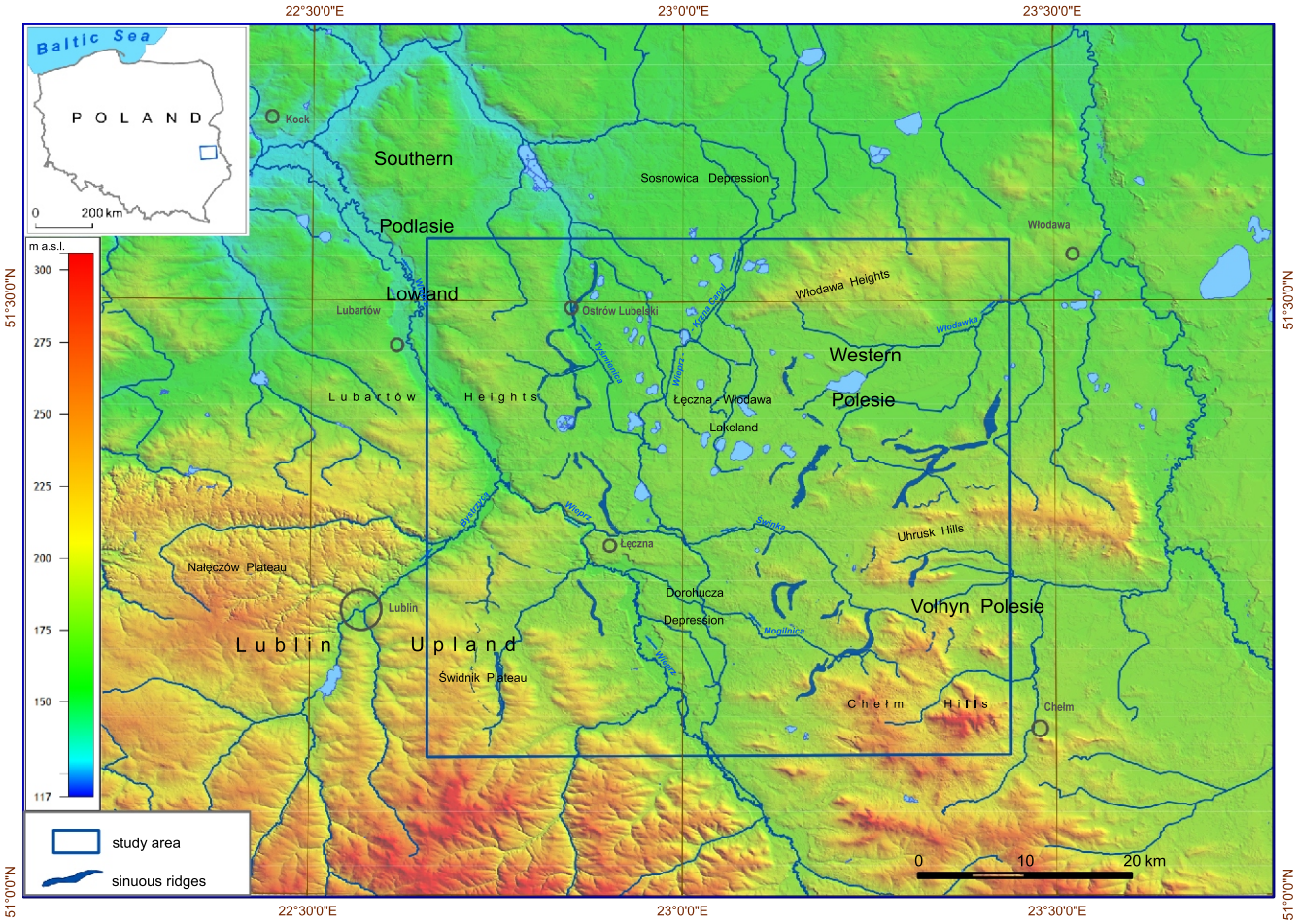

Fig. 2. Location of the study area with sinuous ridges marked

A detailed inventory of inverted channels occurring worldwide was carried out by Zaki et al. (2021). Based on an analysis of the available global literature, satellite image studies and DTM, Zaki et al. (2021) made an inventory of over 100 different inverted channels, dividing them into categories according to their genesis as:

- Channel fill cementation – which were formed by the cementation of deposits filling the channel and its subsequent exhumation.
- Channel fill lithification – which were formed by the lithification of deposits deep below the surface and were then exhumed by tectonic movements and erosion.
- Filling by volcanic materials – where inverted channels were formed by filling the channel with volcanic lava and then its exhumation.
- Channel surface armouring – which was formed by cementation of the channel surface through chemical processes or the formation of a so-called armour of resistant sediments, e.g., gravel and boulders. Its surroundings were degraded, and the armour protected the channel from erosion.

The 4 types of inverted channels listed above cannot, we consider, explain the forms studied in Polesie. Despite their similarity to the forms described from elsewhere in the world, the sinuous ridges found in Polesie were formed differently.

In this paper, we describe the types of inverted channels found at Polesie, and discuss the processes that caused their formation.

STUDY AREA

The study area is located in eastern Poland, in Polesie, in the middle Wieprz River basin, at the junction of four macroregions: Southern Podlasie Lowlands, Western Polesie, Volhyn Polesie and Lublin Upland. The central part of the area is occupied by an extensive plain at an altitude of ~160–170 m a.s.l., cut by the Wieprz River valley and its tributaries, belonging to the Łęczna-Włodawa Lakeland and Dorohucza Depression mesoregions. This flat terrain is surrounded by areas located over 200 m a.s.l.: the Lubartów Heights, Włodawa Heights, Uhrusk Hills, Chełm Hills and Świdnik Plateau (Fig. 2).

Geologically, the study area is located in a zone of high-lying Upper Cretaceous strata (Maastrichtian), mainly comprising chalk, marl, opoka and, as well as gaize and Paleogene calcareous gaize. Opoka rocks are composed mainly of calcium carbonate and organogenic silica, while gaize rocks are siliceous rocks composed mainly of detrital quartz and organogenic silica. These strata underlie flat areas at altitudes of 140–160 m a.s.l., and hilly areas at nearly 200 m a.s.l., and are commonly exposed at the surface. The chalk rocks are overlain by a thin layer of Quaternary deposits ranging from several to several tens of metres in thickness. Only locally, in areas of deep erosion, does the thickness of Quaternary deposits exceed 100 m. The Quaternary succession comprises mainly river, river-floodplain and aeolian deposits from the Middle and Northern Polish Glaciation. There are also glacial and glaciofluvial deposits from the last glaciation, Sanian 2 (Elsterian),

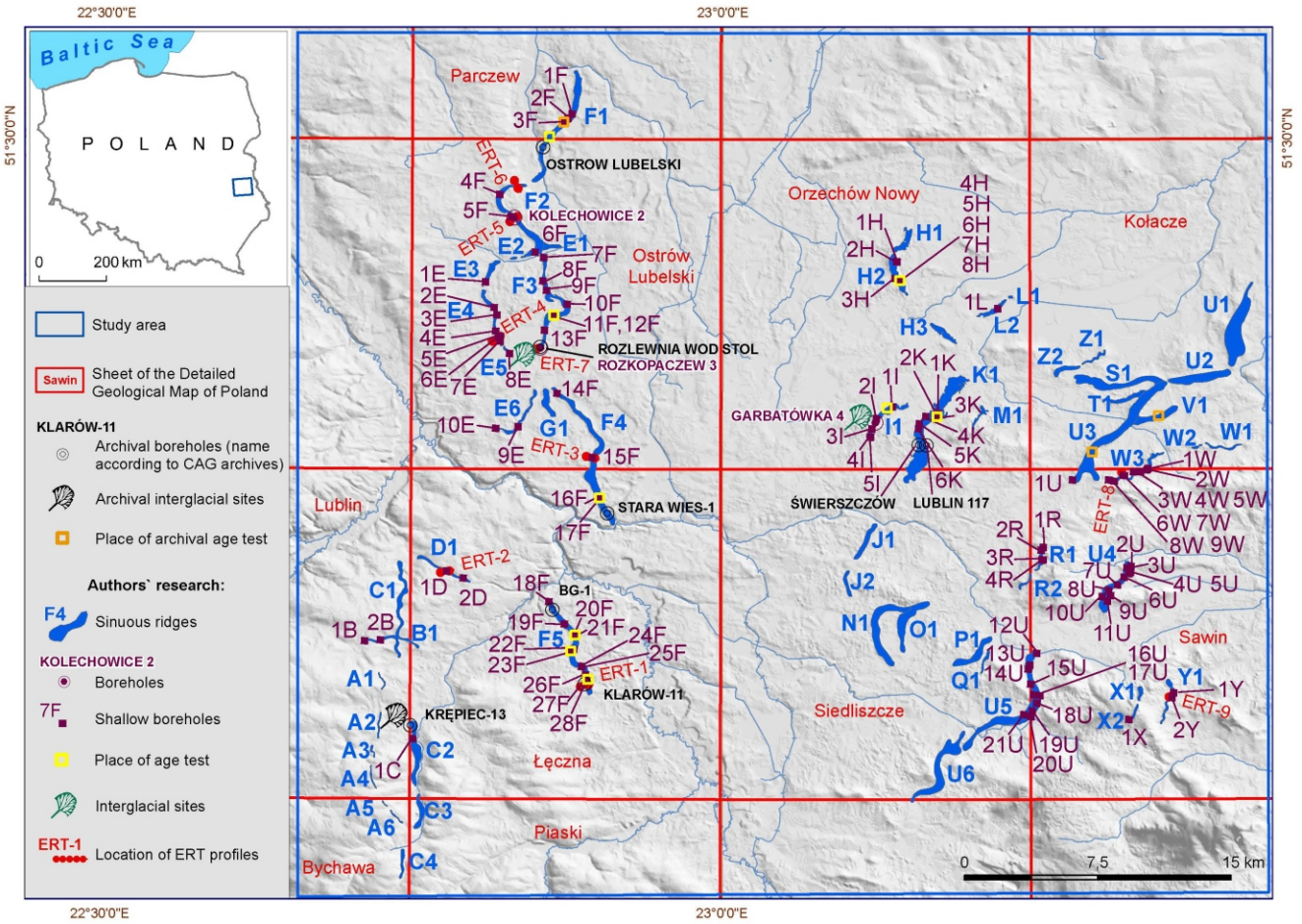

Fig. 3. Map documenting the techniques used for this study

whose ice sheet covered the area in question. These comprise thin covers of glacial clay, glacial sand and fluvioglacial deposits, as well as silts, sands and gravels of postglacial forms such as kames, eskers and terminal moraines.

MATERIALS AND METHODS

Archival geological documentation, including geological photographs, borehole descriptions, geophysical survey results and palynological studies were analysed. Within the boundaries of the sheets of the Detailed Geological Map of Poland that we mapped, field observations were conducted, a number of shallow boreholes were drilled by hand and 3 mechanically, ERT (Electrical Resistivity Tomography) geophysical surveys were carried out as well as laboratory work and palynological and numerical age dating by the OSL (Optically Stimulated Luminescence) method (Fig. 3). This work extended over the following SMGP sheets: Lubartów sheet (Kucharska and Krawczyk, 2023a, b), Łęczna sheet (Krawczyk and Kucharska, 2023a, b), Orzechów Nowy sheet (Kucharska, 2023a, b), Ostrów Lubelski sheet (Krawczyk, 2023a, b) and Sawin sheet (Kucharska, 2025a, b).

Several forms from the study area, located within the SMGP sheets we mapped, were selected for closer analysis. These included forms from sequences E, F, I and K as well as W3 and Y1 (Fig. 3 and see below for explanation of notation). For the remaining forms, only morphometric analyses and in some cases other investigations were conducted.

MORPHOMETRICS OF THE FORMS STUDIED

A thorough DTM analysis was carried out, as well as field surveys from which all forms of sinuous ridge were catalogued (Fig. 3). Each form was given its individual code, which consisted of a capital letter of the alphabet and an Arabic numeral e.g., F1. Forms that we considered were part of a single sequence had the same letter designation and were given another Arabic numeral e.g., F1–F5. Numbering began with the northernmost form. A morphometry of all individual ridge forms was prepared (Table 1). For the morphometric analysis, the relative height of the form (above the surrounding area) at the highest point was measured. The width of the form was measured at 6 locations. Based on this, the arithmetic mean, and standard deviation (?) were calculated for the width parameter. The length of the individual forms (along their axis) was also measured. The morphology of the individual forms was analysed by creating cross-sections at selected characteristic locations (Fig. 4).

For the morphometric analyses, a DTM developed as part of the ISOK project (IT Country Protection System) was used. The DTM was created on the basis of elevation data collected in the form of a point cloud, obtained using the Airborne Laser Scanning (ALS) method.

DATING OF THE DEPOSITS

To determine the age of sedimention, 15 numerical age analyses were carried out using the OSL (Optically Stimulated Luminescence) method performed at the LumiDatis laboratory

in Toruń. Equivalent dose measurements were performed using the standard SAR OSL (Single Aliquot Regenerative Dose Optically Stimulated Luminescence) method (Krawczyk, 2023a; Krawczyk and Kucharska, 2023a; Kucharska, 2023a; Pochocka-Szwarc, 2023; Żarski, 2023).

Additionally, palynological and palynostratigraphic studies were performed. Archival research (Janczyk-Kopikowa, 1981) and new research that was carried out as part of the SMGP mapping exercise (Krawczyk, 2023a; Krawczyk and Kucharska, 2023a; Kucharska, 2023a) were used. Organogenic deposits which had plant taxa in their composition were studied. The study material came from hand and mechanical drilling.

GEOPHYSICAL SURVEYS

Geophysical surveys performed for the SMGP implementation were used for depth profiling (Pacanowski 2021; Krawczyk and Kamiński, 2024). As part of the work, nine Electrical Resistivity Tomography (ERT) profiles were made transverse to the ridge long axes (Pacanowski, 2021; Krawczyk and Kamiński, 2024), where a gradient measurement system was used (Fig. 3). Electrofusion tests were carried out using the Roll Along method with electrode spacing at 10 m intervals – moving successive cables to the front of the profile, which allowed for longer, continuous profiles. A set of cables on spools containing 21 leads was used. The survey data was analysed using Res2DINV software. Characteristic ridges pre-designated as inverted fluvial channels from sequences F, E and G, as well as ridges W and Y, whose structure could indicate a post-glacial origin, were selected for the geophysical survey. The research was aimed at identifying not only the depth structure beneath the forms in question, but also that of the areas in the vicinity of the ridges. We aimed to better constrain the boundary between Cretaceous and Paleogene rocks and Pleistocene deposits. The profiling reached a depth of ~150 m at its deepest point in ERT cross-sections 1–6, and ~80 m in ERT cross-sections 7–9.

GEOLOGICAL STRUCTURE OF THE FORMS STUDIED

For analyses of geological structure of the ridge forms, we used our own fieldwork results, carried out as part of updating four sheets of the Detailed Geological Map of Poland (SMGP) at 1:50000 scale: the Łęczna (Krawczyk and Kucharska, 2023a, b), Orzechów Nowy (Kucharska, 2023a, b), Ostrów Lubelski (Krawczyk, 2023a, b) and Sawin (Kucharska 2025a, b) sheets. The superficial ridge geological structure of the ridge was recognised by digging shallow trenches and shallow manual boreholes in accessible places, reaching a maximum depth of ~4 m, and by describing natural exposures. One hundred such documentation points were made. The lithological variation in the profiles of these boreholes and exposures was described using a lithofacies code to identify individual sedimentary changes, where: F – silt, S – sand, G – gravel, D – diamicton and combinations of individual lithologies by e.g., FS – sandy fines or SG – gravelly sands. Additionally, sediment structures have been recorded: m – massive structure, h – horizontal lamination, f – flaser lamination, t – trough cross-stratification (Zieliński, 1995; Zieliński and Pisarska-Jamroży, 2012).

Due to the limited capacity and scope of the subject, the most characteristic ridges in the study area were selected for the pilot geological reconnaissance work. These were the ridge sequences E, F, I and K as well as W3 and Y1.

On the ridges F2, F3 and I1, mechanical boreholes were drilled: Kolechowice 2, Rozkopaczew 3 and Garbatówka 4 (Fig. 3).

Archival profiles of geological boreholes were used to constrain the geological structure of the ridges and of the underlying strata. These boreholes are Ostrów Lubelski, Rozlewnia Wód Stol, Stara Wieś-1, Krępiec-13, Klarów-11, Świerszczów and Lublin 117 (names according to Central Geological Archive – CGA archives).

To determine the genesis of the forms in question, archival borehole profiles were analysed for carbonate rocks and rocks containing clay minerals. The mechanical properties of the rocks found in the study area may contribute to the specific conditions for the formation of the sinuous ridges. An important factor influencing the form of the sinuous ridges is the phenomenon of swelling and shrinkage of sediments due to wetting and drying. We considered this factor for the Maastrichtian and Paleogene, as well as the Pleistocene, deposits of the area.

RESULTS

MORPHOMETRICS OF THE FORMS STUDIED

The ridge forms under investigation have specific orientations running N–S, NW–SE and NE–SW. Their arrangement reveals patterns, such as that of forms F, which runs from Ostrów Lubelski in the north to the vicinity of Łęczna (Fig. 2). In the eastern part of the area, the forms are more scattered, which does not allow them to be clearly connected into coherent patterns.

Due to their relatively low relative heights, the sinuous ridges are not very distinct and are poorly visible in the terrain. Topographic maps also do not show their full shape, but only indicate small hills, the distribution of which does not always reveal a coherent system. This may have been the reason for the poor recognition of these forms in the past.

The subsequent availability of digital terrain models allowed thorough analysis of the morphology of the study area and the identification of individual morphological forms. Thanks to the use of elevation data characterised by a very high measurement accuracy of several tens of centimetres, sinuous ridges were identified and analysed (Fig. 4).

Based on the DTMs, the morphometries of 57 ridge forms in the study area were selected and analysed. The results are shown in Table 1

These measurements showed that the average height of the forms is 3.6 m (Tables 1 and 2). The lowest form is 0.4 m (A5), and the highest is 8.2 m high (U3). The average width of the forms is 235.5 m (standard deviation is 52.21 m). The lowest average form width is 69.6 m (A5), and the highest average width is 584.1 m (K1). The average length of the forms is 3135.9 m. The shortest form is 236.7 m long (L1), and the longest extends over a distance of 9346.0 m (F4).

DATING OF RIDGE DEPOSITS

To determine the age of the deposits of the forms selected, OSL dates were obtained, as used in the making of SMGP maps (Żarski, 2023; Pochocka-Szwarc, 2023; Fig. 3), Ostrów Lubelski (Krawczyk, 2023a, b), Orzechów Nowy (Kucharska, 2023a, b), Łęczna (Krawczyk and Kucharska, 2023a, b), and Sawin (Kucharska, 2025a, b).

Three OSL dates were obtained from the F1 ridge: at point 3F, at a depth of 1.2 m, a date of 14.3 ±2 kyr was obtained, and south of point 3F, at a depth of 1.45 m, a date of 19.0 ±3 kyr was obtained, and at a depth of 2.3 m, a date of 72.0 ±15 kyr was obtained.

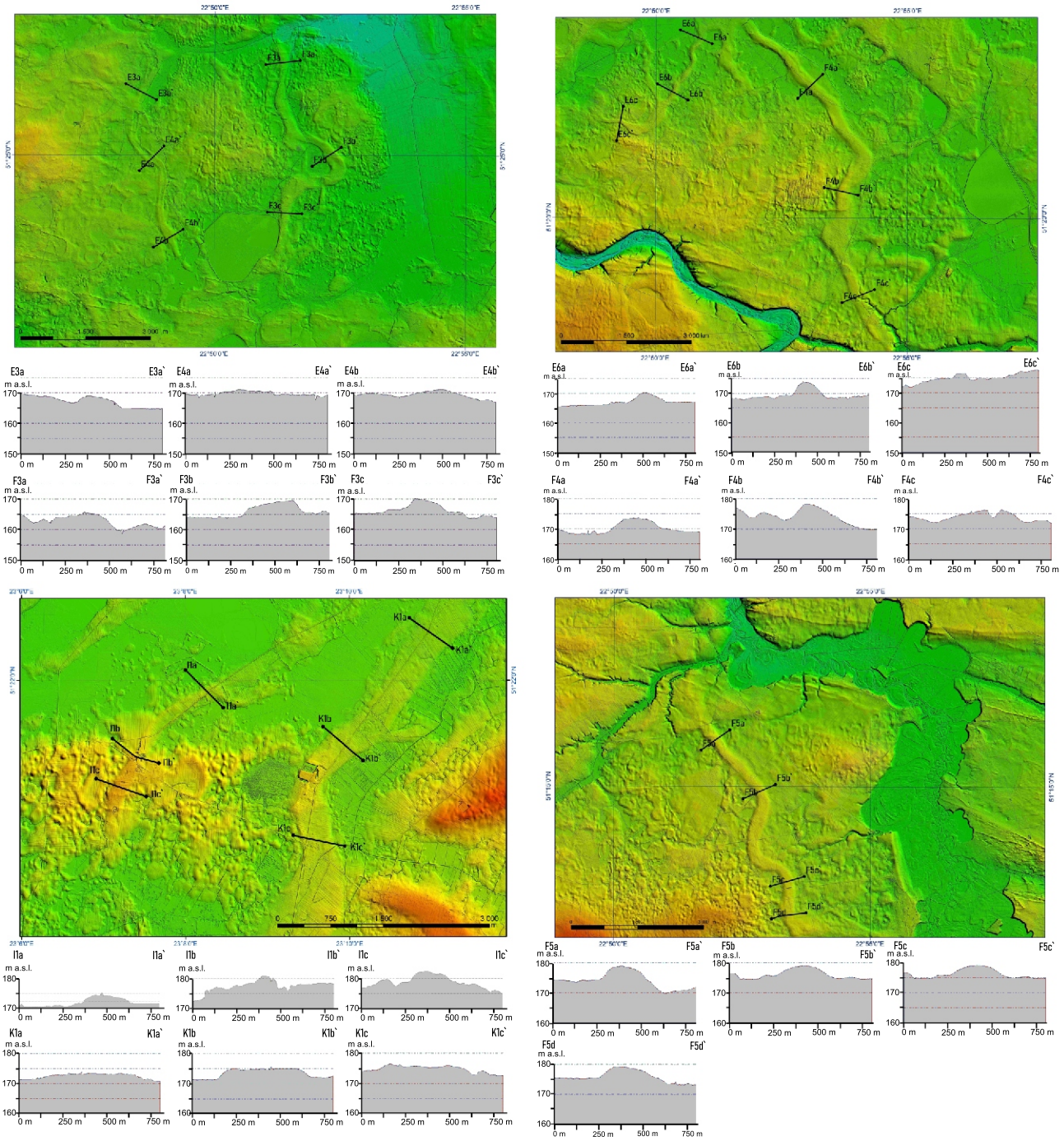

Fig. 4. Cross-sections through selected sinuous ridges

The deposits of ridge F3 were dated at point 12F, obtaining a date of 13.5 ±2.2 kyr at a depth of 1.2 m, and those from ridge F4 at a depth of 1.1 m yielded a date of 16.3 ±3.3 kyr.

The best OSL dating results were obtained for ridge F5, from whose deposits five dates were obtained. At point 20F, from a sample taken at a depth of 1.9 m, a date of 29.0 ±1.9 kyr was obtained. At point 23F, above organic deposits, a date of 7.0 ±2.9 kyr was obtained at a depth of 1.0 m, and of 39.0 ±11.3 kyr at a depth of 2.4 m. From point 28F, a sample taken at a depth of 1.4 m yielded a date of 13.2 ±2.8 kyr, and one from a depth of 2.0 m gave a date of 16.3 ±2.8 kyr.

On ridge I1, at point 1I, a date of 13.8±2.7 kyr was obtained from a depth of 1.1 m. On ridge K1, a date of 91.0±14 kyr was obtained from a depth of 1.4 m.

All these dates indicate sedimentation throughout the Vistulian and early Holocene (Table 3). However, the accumulation of results within the range of 12–19 thousand years clearly indicates increased sedimentation in the late glacial period.

On ridge H2 at point 7H, a date of 210.0 ±50 kyr was obtained at a depth of 1.0 m, indicating sedimentation during the Odranian glaciation or Mazovian interglacial period. On the U3 ridge, a date of 180.0 ±30 kyr was obtained from a depth of

Table 1

Measurements of sinuous ridge morphometry in the study area

Sinuous ridge	Width (m)											height (m)	length (m)
	measurement						sum	average width	standard deviation σ	min	max		
	1	2	3	4	5	6							
A1	69.8	78.4	86.1	78.4	88.4	83.3	484.4	80.7	6.1	69.8	88.4	1.1	1 156.2
A2	95.0	83.4	88.7	79.5	81.7	99.6	527.9	88.0	7.3	79.5	99.6	2.1	1 509.3
A3	140.3	113.2	118.4	66.0	65.0	93.5	596.4	99.4	27.6	65.0	140.3	1.6	805.7
A4	69.9	66.1	76.0	114.3	63.8	77.8	467.9	78.0	17.0	63.8	114.3	1.4	1 422.0
A5	76.4	82.2	53.1	66.8	65.1	74.1	417.7	69.6	9.4	53.1	82.2	0.4	458.1
A6	70.8	80.4	101.0	66.0	70.3	94.5	483.0	80.5	13.1	66.0	101.0	1.7	1 534.6
B1	99.1	104.0	138.5	126.1	143.0	145.1	755.8	126.0	18.3	99.1	145.1	1.7	3 442.1
C1	281.9	152.0	217.1	165.2	151.4	320.0	1287.6	214.6	65.8	151.4	320.0	2.5	5 888.4
C2	419.2	242.6	199.4	277.3	369.1	515.3	2022.9	337.2	108.8	199.4	515.3	0.9	3 789.4
C3	144.9	192.8	261.7	282.1	297.2	299.2	1477.9	246.3	57.8	144.9	299.2	0.7	2 154.0
C4	202.5	223.6	143.5	121.8	145.2	107.2	943.8	157.3	41.9	107.2	223.6	2.2	1 722.8
D1	197.1	153.1	146.2	135.8	126.5	138.0	896.7	149.5	22.9	126.5	197.1	1.8	3 377.7
E1	95.0	128.5	276.7	301.1	233.1	191.9	1226.3	204.4	74.5	95.0	301.1	3.8	2 445.5
E2	111.7	121.1	129.6	138.9	152.4	132.9	786.6	131.1	12.9	111.7	152.4	2.2	422.7
E3	239.9	222.9	363.9	347.1	227.6	208.9	1610.3	268.4	62.5	208.9	363.9	1.6	1 819.0
E4	228.4	184.0	198.0	235.7	161.3	213.6	1221.0	203.5	25.7	161.3	235.7	2.3	3 555.3
E5	113.5	129.9	133.1	131.3	67.7	38.9	614.4	102.4	36.3	38.9	133.1	2.7	683.2
E6	210.0	125.1	151.3	108.4	127.1	120.3	842.2	140.4	33.7	108.4	210.0	4.8	4 100.1
F1	234.6	337.8	379.4	448.8	314.3	318.5	2033.4	338.9	65.3	234.6	448.8	5.3	7 339.0
F2	190.5	227.9	97.1	245.8	301.5	297.9	1360.7	226.8	69.7	97.1	301.5	5.4	6 063.6
F3	292.3	201.9	101.8	289.6	274.7	166.0	1326.3	221.1	71.0	101.8	292.3	6.1	7 062.0
F4	214.1	182.5	326.9	192.7	289.5	348.7	1554.4	259.1	65.6	182.5	348.7	6.2	9 346.0
F5	306.1	305.7	293.6	361.1	275.6	344.1	1886.2	314.4	29.3	275.6	361.1	6.4	6 303.5
G1	330.3	326.7	459.6	269.5	243.5	285.2	1914.8	319.1	69.8	243.5	459.6	4.6	1 776.1
H1	356.8	325.3	306.6	347.1	337.4	345.7	2018.9	336.5	16.5	306.6	356.8	4.8	1 756.0
H2	347.6	453.5	585.8	438.7	338.5	270.6	2434.7	405.8	101.6	270.6	585.8	4.9	2 548.2
H3	214.2	299.2	325.4	387.9	289.8	165.7	1682.2	280.4	72.5	165.7	387.9	0.9	1 885.9
I1	206.5	116.6	241.1	264.2	259.4	256.4	1344.2	224.0	51.7	116.6	264.2	3.2	3 496.7
J1	275.3	242.6	278.4	277.0	269.1	260.1	1602.5	267.1	12.6	242.6	278.4	1.8	2 398.5
J2	194.6	198.3	175.6	214.7	174.4	172.9	1130.5	188.4	15.4	172.9	214.7	1.3	1 607.5
K1	477.9	920.3	641.6	431.3	423.8	609.6	3504.5	584.1	171.9	423.8	920.3	4.2	7 201.6
L1	173.5	159.6	154.7	156.9	157.0	154.9	956.6	159.4	6.5	154.7	173.5	1.6	236.7
L2	123.1	177.3	186.0	209.3	290.0	309.3	1295.0	215.8	64.9	123.1	309.3	5.6	1 978.0
M1	180.5	168.8	121.6	103.3	82.1	177.1	833.4	138.9	38.5	82.1	180.5	2.3	1 604.3
N1	270.6	375.5	385.2	356.0	449.1	390.9	2227.3	371.2	53.3	270.6	449.1	5.1	5 242.5
O1	343.4	360.1	359.6	552.1	505.4	450.5	2571.1	428.5	79.9	343.4	552.1	1.3	3 696.5
P1	276.2	311.4	342.5	238.6	416.5	432.2	2017.4	336.2	70.1	238.6	432.2	3.2	2 916.4
Q1	156.2	165.1	165.2	220.0	101.5	99.1	907.1	151.2	41.5	99.1	220.0	3.2	1 426.1
R1	115.2	106.6	104.5	183.1	189.9	121.4	820.7	136.8	35.6	104.5	189.9	5.1	1 742.2
R2	123.4	104.2	93.4	93.9	131.0	153.4	699.3	116.6	21.7	93.4	153.4	2.2	1 298.7
S1	367.4	267.8	288.3	306.5	317.1	228.7	1775.8	296.0	42.9	228.7	367.4	4.9	5 028.0
T1	391.5	250.2	245.2	231.4	194.3	228.2	1540.8	256.8	62.8	194.3	391.5	6.3	2 100.6
U1	141.8	473.4	542.1	652.3	645.9	675.2	3130.7	521.8	184.0	141.8	675.2	5.7	5 043.5
U2	364.6	373.7	380.6	472.9	500.7	509.5	2602.0	433.7	61.9	364.6	509.5	6.6	3 603.0
U3	307.6	450.5	461.6	399.5	504.8	489.4	2613.4	435.6	66.2	307.6	504.8	8.2	7 938.0
U4	335.2	456.2	459.5	282.2	247.5	296.9	2077.5	346.3	83.0	247.5	459.5	4.2	3 446.0
U5	342.8	457.3	385.3	447.3	296.6	416.6	2345.9	391.0	57.0	296.6	457.3	3.5	8 420.3
U6	228.9	169.6	819.8	263.7	283.9	291.2	2057.1	342.9	217.1	169.6	819.8	3.1	5 738.9
V1	377.4	361.4	365.1	325.0	275.3	269.6	1973.8	329.0	43.1	269.6	377.4	4.9	2 482.0
W1	81.9	97.0	85.9	138.0	82.9	159.8	645.5	107.6	30.3	81.9	159.8	3.1	2 276.0
W2	93.1	47.2	68.9	142.7	134.5	108.2	594.6	99.1	33.9	47.2	142.7	2.8	644.5
W3	95.2	146.6	200.4	224.6	185.8	121.6	974.2	162.4	45.3	95.2	224.6	4.9	4 393.4
X1	274.4	295.3	234.1	210.9	161.6	151.8	1328.1	221.4	53.2	151.8	295.3	4.7	854.3
X2	118.0	126.8	147.2	140.4	131.3	169.8	833.5	138.9	16.7	118.0	169.8	3.1	1 194.4
Y1	281.0	301.3	115.3	192.1	110.2	90.5	1090.4	181.7	83.8	90.5	301.3	4.5	2 953.6
Z1	160.6	143.5	112.8	91.6	166.3	118.2	793.0	132.2	26.8	91.6	166.3	7.8	1 728.6
Z2	161.8	217.2	229.5	260.6	258.2	257.5	1384.8	230.8	34.9	161.8	260.6	5.7	1 686.5

1.0 m, and on the V1 ridge, a date of 200 ±60 kyr was obtained. These dates also indicate sedimentation during the Odranian glaciation or the Mazovian interglacial period (Table 3).

Palynological and archival palynological studies have allowed indirect dating of deposits found in depressions beneath the ridges. In all three boreholes drilled during our research, located on sinuous ridges, deposits containing organic matter were encountered.

In boreholes Rozkopaczew 3 at a depth of 9.2 m and Garbatówka 4 at a depth of 3.9 m (Figs. 3 and 7) deposits containing organic matter were drilled. Preliminary palynological analysis showed that these belong to the second half of the Mazovian interglacial (Krawczyk, 2023a; Kucharska, 2023a). In the third borehole, Kolechowice 2, no plant pollen was found, and the deposit was classified as of cold lake type (Krawczyk, 2023a, b).

In the Krępiec-13 archive borehole (Figs. 3 and 8), deposits found at depths ranging from 8.9 m to 41.5 m are classified as belonging to the Mazovian interglacial. The entire profile of lake deposits is considered to be a stratotype profile of this interglacial (Janczyk-Kopikowa, 1981; Krawczyk and Kucharska, 2023a, b).

GEOPHYSICAL SURVEYS

As part of the mapping for the SMGP, nine ERT cross-sections of the ridges were made (Fig. 3; Pacanowski, 2021; Krawczyk and Kamiński, 2024). These were sited along eight sinuous ridges (two ERT cross-sections were performed on ridge F2). The values obtained indicate the presence of zones under the ridges with clearly different resistivities compared to the adjacent areas. These zones were most often U-shaped depressions formed in the Quaternary subsoil. The resistivity of the shallow subsoil, composed mainly of marl, chalk and opoka, ranges from 20 to 40 m (Fig. 5).

On the **F5** ridge, the ERT-1 geoelectric section is located, in its southern part, in the area of the Klarów-11 archival borehole. The resistivity distribution pattern shows little variation (Fig. 5). Under the axial part of the ridge, a zone of increased resistivity (~100 m) is faintly visible at a depth of ~40–60 m. Similar zones of increased resistivity can be observed at depths of ~50–100 m in its eastern and western parts. The Klarów-11 borehole profile documents the presence of very thick (>80 m) clayey and silty deposits in this area, whose resistivity parameters are similar to those of the Cretaceous strata beneath the Quaternary deposits. This convergence of resistivity parameters in this case may partially obscure the geological structure.

On the **D1 ridge**, an ERT-2 electrical resistivity profile was made. This profile documents the occurrence of a well-defined U-shaped zone under the ridge with high resistivity (close to 200 m) to >20 m depth and less well-defined to >50 m depth (Fig. 5). The width of this zone is ~125 m.

The ERT-3 cross-section is located in the central part of the **F4** ridge. Here, a zone of increased resistivity (over 100 m) is marked under the ridge over a width of ~400 m in the western part to a depth of ~45 m and in the eastern part to a depth of 55 m (Fig. 5).

An ERT-4 cross-section was located on ridge **E4**. Over a distance of ~130 m, its profile shows a zone with significantly increased resistivities (Fig. 5). To a depth of 35.0 m, resistivities range from 100 m to >200 m. The highest resistivity values of ~250 m in this zone were recorded in its central part. Below this zone, to a depth of ~80 m, there is a decrease in resistivity from 10 to 60 m. To a depth of ~100 m, resistivity increases again to ~100 m.

Table 2

Average values of sinuous ridge morphometry measurements

	average (m)	min (m)	max (m)	standard deviation
form height	3.6	0.4	8.2	
form width	235.5	38.9	920.3	52.2090
form length	3135.9	236.7	9346.0	

Two cross-sections were made on the northern part of the **ridge F2**: ERT-5 and ERT-6. In the ERT-5 cross-section, a depression reaching >100 m and nearly 350 m wide is clearly visible under the ridge (Fig. 5). The depression is marked by increased resistivity to >100 m. The ERT-6 cross-section shows a depression ~380 m wide with significantly higher resistivity than the surrounding area. It reaches a depth of ~60 m (Fig. 5).

On the **F3** ridge, the ERT-7 cross-section was made across the southern part of the ridge, in the area of the Rozkopaczew 3 borehole. Under the ridge, there is a clear depression filled by deposits with resistivity values exceeding 100 m (Fig. 6). The chalk substrate at this location is characterised by resistivity values within the range of 20 m. Due to infrastructure (roads, buildings), the ERT-7 sequence could not be longer than 400 m; therefore, the measurements did not reach the bottom of the depression. The depression may exceed a depth of 100 m.

An ERT-8 cross-section was made on the **W3** ridge. Here, a very high U-shaped zone of high resistivity up to >400 m, and locally up to >600 m, is clearly visible (Fig. 6). This zone extends to a depth of ~30 m. Such high resistivity can be associated with dry, coarse-grained deposits such as sand, gravel and boulders. This sedimentary lithology may indicate a post-glacial origin of the **W3** form.

A similar situation to that on ridge **W3** occurs on ridge **Y1**. Here, an ERT-9 cross-section was made. Very high resistivity values of over 600 m to a depth of ~40 m indicate that the ridge and the channel are filled with coarse-grained deposits, which may also indicate the glacial origin of the Y1 form (Fig. 6).

Geophysical surveys in the ridge areas allowed for the separation of Maastrichtian and Paleogene strata from Quaternary deposits. As shown by electrical measurements, U-shaped depressions occur below all the ridges studied, as indicated by higher resistivities of 60–600 m, reaching depths of 30–100 m. These depressions differ from the chalk substrate, resistivities of which range from 20 to 40 m (Pacanowski, 2021; Krawczyk and Kamiński, 2024; Figs. 5 and 6). Such a distribution of resistivities may corroborate the presence of erosional valleys beneath the sinuous ridges analysed.

The resistivity distribution in the W and Y forms and in the depressions beneath them is homogeneous and ranges between 400 and 600 m. The depressions reach a depth of ~30–40 m. This indicates a homogeneous geological structure of the forms and depressions beneath them. They are composed of coarse-grained deposits such as sand, gravel and boulders. Therefore, we associate these ridges with glacial forms.

In other forms of D, E, and F, classified by the authors as inverted fluvial channels, the resistivity distribution in the ridges and in the zones below them ranges from 20 to 100 m. The resistivity distribution documents much deeper depressions than

Table 3

Stratigraphy of the Quaternary (Lindner and Marks, 2008, modified; Marks, 2023, modified; marine isotope stages – MIS)

Stratigraphy						MIS	Age kyr
Holocene						1	11,7
Pleistocene	Upper	North Polish Complex	Vistulian	Late Glacial	Younger Dryas	2-5d	15
					Allerød		
					Older Dryas		
					Bølling		
					Oldest Dryas		
				Plenivistulian			70
				Early Vistulian			
			Eemian			5e	115
	Middle	Middle Polish Complex	Odranian			6-10	129
			Mazovian			11c	
		South Polish Complex	Sanian 2			12	424
			Ferdynandovian			13-15	
			Sanian 1			16	621
			Podlasian			17-19(21)	774
	Lower		Nidanian			20(22)	900
		Augustovian				21-25(27)	
		Oldest Glaciation (Narevian)				26-28(30)	

in ridges W and Y, reaching up to 100 m. Resistivities within the range of 20–100 m indicate that the depressions are filled with fine-grained deposits such as sand, silt, clay and organic matter. Low resistivities may indicate the presence of water in the deposits.

GEOLOGICAL STRUCTURE OF THE FORMS STUDIED

Two genetic types were identified among all the sinuous ridges studied: glacial forms and inverted fluvial channels. Some of the sinuous ridges were classified as glacial forms at the initial stage of the work. These are the W and Y forms. They are composed of coarse sedimentary deposits, sands and gravels with interlayers of sand and silt, indicating high variability in the sedimentation dynamics. On their surfaces and in their vicinity, gravel and boulders ranging from 5 to 20 cm across and flint cobbles up to 10 cm in size may be found. Here and there, boulders of northern rocks with diameters of 0.5–1.0 m occur. The deposits in their upper part have a massive structure, with horizontal layering below. Locally, there is evidence of post-depositional disturbance, with normal faults that may indicate sedimentary disturbances during ice retreat. The high variability of grain size and sedimentary structure indicates sedimentation in ice cracks.

The remaining sinuous ridges were classified with high probability as **inverted fluvial channels**. Their documented geological features indicate a characteristic geological structure indicating fluvial and lacustrine sedimentation. The forms in question are mainly composed of fine-grained deposits (Table 4). These comprise alternating layers of fine- and medium-grained sands (S), silts and clays (F) or combinations of these lithologies: silty sands and silty clays (SF) and silts and sandy silts (FS). No coarse-grained deposits or northern-sourced gravels were observed on the surface of the forms. Locally, sedimentary interlayers with organic matter were found in the deposits (Table 4). On the slopes of the ridges forms, faults from subsidence are locally encountered in the deposits (Liszkowski, 1979a).

On ridge F5, layers with a distinct organic content were penetrated by hand drilling (Table 4): at point 21F at a depth of 2.1–3.0 m, at point 22F at a depth of 1.7–2.2 m, at point 23F at a depth of 2.5–3.9 m, at point 24F at a depth of 1.8–3.0 m, at point 25F at a depth of 2.2–3.1 m (Fig. 3). Samples for palynological analysis were taken from these layers at points 21F and 23F. Due to the poor preservation of sporomorphs and their small quantity, palynological analysis did not allow the age of the sediment to be determined. They only indicated derivation of material from land and its redeposition (Krawczyk and Kucharska, 2023a).

Based on shallow drilling, it was found that the U4 ridge has a completely different geological structure (Fig. 3). In the upper part of the form, silty sands (SF), sandy silts (FS) and sands (S) were found at almost all points to a depth of ~1.5 m. This is documented by sample profiles at points 6U and 10U (Table 4). These deposits contain fine gravel or clay interlayers. Below them, there is glacial clay (Dm), documented at points 6U, 8U and 10U, reaching a depth of 3.0 m at point 8U. Ridge U4 requires further research and analysis.

RESEARCH BOREHOLES

There are a few archival boreholes on the ridges. These document deep depressions located under the ridges (Fig. 7), which were classified by Kucharska et al. (2024) as subglacial troughs. The troughs are filled with clastic deposits, mostly fine-grained: silt, fine-grained sand and medium-grained sand predominate. These troughs are incised in Maastrichtian rocks.

As part of our own work, three exploratory boreholes were drilled, located on ridges F2, F3 and I1, to investigate the deep geological structure. These showed the presence of depressions formed in Cretaceous (Maastrichtian) strata beneath the ridges (Fig. 8). In two boreholes, Rozkopaczew 3 and Garbatówka 4, organic layers were drilled among fine-grained deposits; they were subjected to palynostratigraphic analysis (Krawczyk, 2023a; Kucharska, 2023a). Palynological studies allowed determination of their age as Mazovian (Holsteinian). In the Kolechowice 2 boreholes, fine-grained sandy silt and silt deposits were drilled to a depth of 18 m. Preliminary palynological analysis showed no sporomorphs that might allowing estimation of their age (Krawczyk, 2023a). By analogy with the occurrence of organic deposits in the boreholes Rozkopaczew 3 and Garbatówka 4, we correlated these deposits with the Mazovian interglacial (Fig. 8). Above these lie river and lake deposits we classified as of Odranian (Saalian) age, while the deposits forming the surface of the ridges belong to the Vistulian and partly to the Holocene.

EROSIONAL TROUGHS

By analysing archival geological boreholes, our own boreholes at Kolechowice 2, Rozkopaczew 3 and Garbatówka 4, as well as archival geophysical studies (Pawłowska and Tracz, 1975) and new (Pacanowski, 2021; Krawczyk and Kamiński, 2024), the occurrence of deep, relatively narrow depressions in the form of erosional troughs were found under the ridge forms. An analysis of the erosional troughs in the study area was made by Kucharska et al. (2024); they may partly run along today's

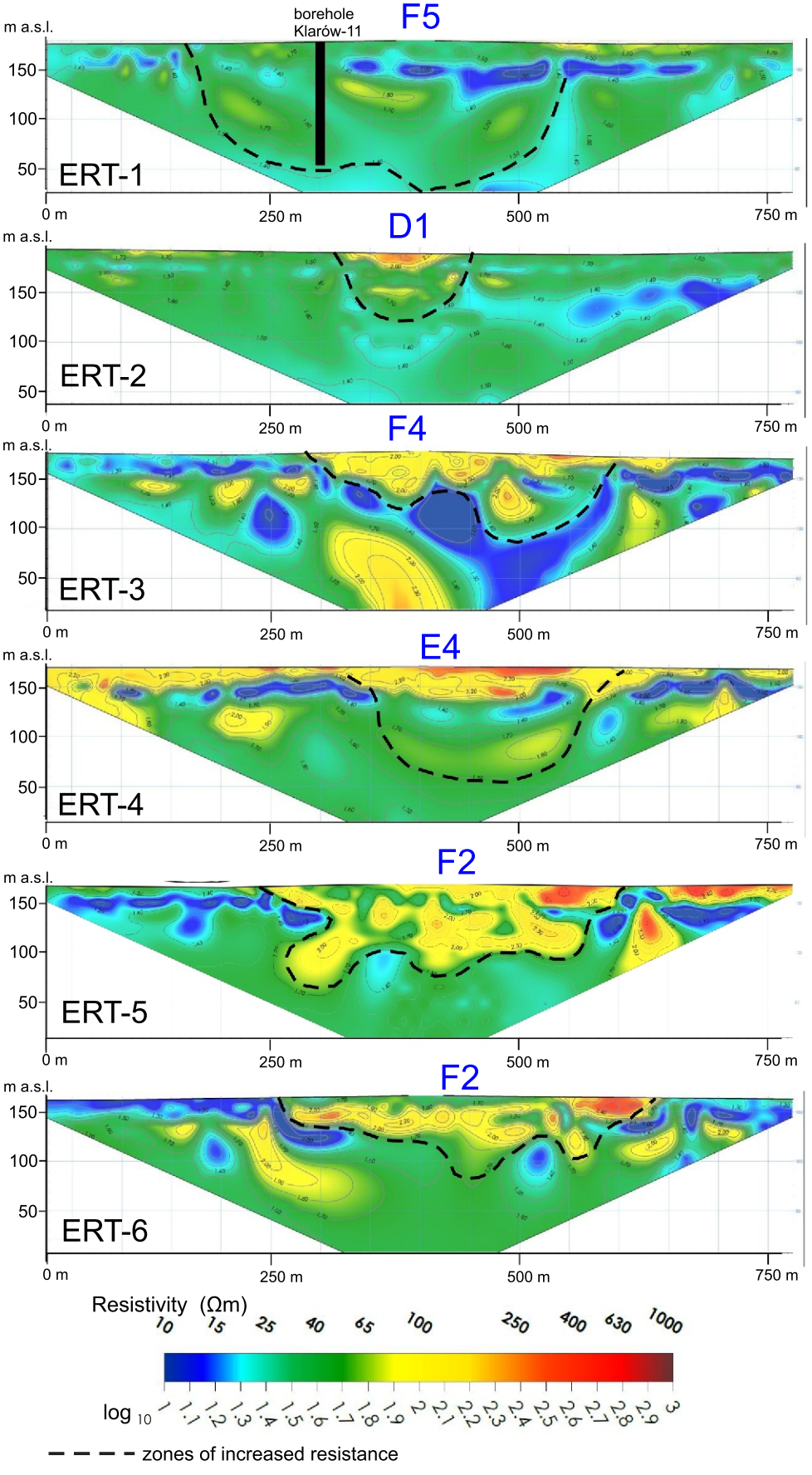

Fig. 5. ERT cross-sections made during the implementation of the SMGP (Pacanowski, 2021, modified)

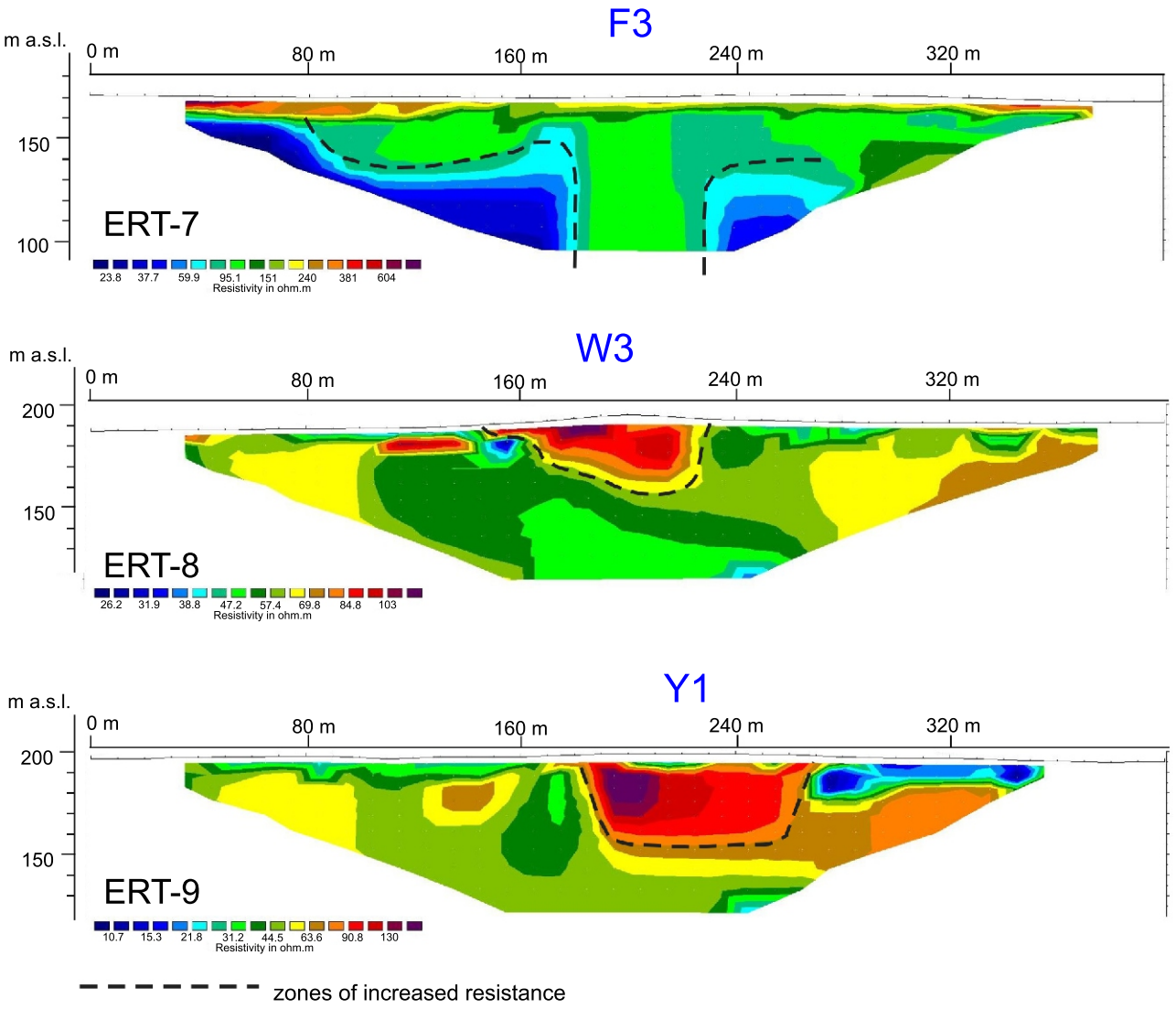

Fig. 6. ERT cross-sections obtained during SMGP realisation (Krawczyk and Kamiński, 2024, modified)

valley depressions and partly overlap with the surface ridges. The trough depressions were incised into Upper Cretaceous strata of the Maastrichtian. In the area of ridges E and F, these strata are mainly of chalk with interlayers of marl and opoka (Liszkowski, 1979a, b; Harasimiuk and Henkiel, 1980a, b; Krawczyk, 2023a, b; Krawczyk and Kucharska, 2023a, b), and in the area of ridges I and K, marl with interlayers of chalk and opoka (Buraczyński and Wojtanowicz, 1981a, b; Kucharska, 2025a, b).

SWELLING

Our analysis of available archival materials showed that the deposits forming the ridges, as well as those occurring in the troughs beneath them, are mainly fine-grained sediments with a high proportion of clay. Deposits of this type have a high water retention capacity due to their clay particles. The troughs, on the other hand, are eroded into carbonate rocks, which are mainly marl, chalk and opoka. Carbonate rocks are therefore found in the immediate vicinity of the ridges, both at the surface or overlain by a thin clastic layer, as well as on the sides of the troughs and in their substrate (Kucharska et al., 2024; Figs. 7 and 8).

The lithologies most susceptible to swelling are cohesive and clay-rich, in particular with minerals of the smectite group. The swelling capacity increases with increasing clay content (Myślińska, 1996; Grabowska-Olszewska, 2004).

In the troughs analysed for which drilling documentation is available, thick layers of clayey and silty deposits were found (Figs. 7 and 8).

Based on available data e.g., from drilling in Krępiec-13 (ridge C2), where a 19-m layer of diatomaceous earth was documented, or in the Klarów-11 borehole (ridge F5), where containing a lot of calcium carbonate lake silts and clays with a thickness of over 70 m occur (Harasimiuk and Henkiel, 1980a, b; Fig. 7), it can be assumed that the sediments filling the troughs have high water absorption capacity and, consequently, are prone to strong swelling and to becoming more plastic. Such properties of the lithologies filling the troughs and of the surrounding rocks cause them to be susceptible to changes in volume and internal structure under the influence of changing hydrogeological conditions.

Table 4

Simplified lithological descriptions of selected documentation points, shallow boreholes

Shallow borehole	Depth; (m)	Deposits
2B	0.0–1.0	Silts, massive structure, light brown
	1.0–1.2	Fine-grained sands and silts, massive structure, light brown
	1.2–2.0	Varied-grain sands, massive structure, light brown
	2.0–2.3	Clayey sands with gravels, massive structure, yellow
	2.3–3.2	Silty sands, massive structure, yellow
	3.2–4.0	Sandy clays with gravels up to 2 cm, massive structure, light grey
	4.2–4.6	Clayey silts, massive structure, grey-brown
1C	0.0–1.0	Silts, massive structure, light brown
	1.0–1.7	Clayey sands with gravels, massive structure, yellow
	1.7–1.8	Silts, massive structure, yellow
	1.8–2.1	Fine-grained sands, massive structure, brown
	2.1–3.1	Fine-grained sands with interbeds of silts with organic matter, yellow
	3.1–3.3	Silts, massive structure, yellow
1D	0.0–1.1	Silts, massive structure, yellow
	1.1–1.3	Varied-grain sands with gravels up to 2 cm, massive structure, light brown
	1.3–3.2	Clayey gravels, massive structure, rusty
1E	0.0–0.5	Silts, clayey silts, massive structure, yellow
	0.5–1.0	Clayey sands, massive structure, brown
	1.0–1.6	Varied-grain sands, slightly silty, single gravels 1–2 cm, massive structure, yellow-brown
	1.6–1.9	Sandy clays, single gravels at base, massive structure, yellow
	1.9–2.0	Varied-grain sands, slightly silty, massive structure, yellow
	2.0–2.3	Sandy silts, massive structure, grey
	2.3–2.7	Medium- and coarse-grained sands, massive structure, yellow
4E	0.0–1.2	Clayey sands, massive structure, light yellow
	1.2–2.4	Sandy clays with individual gravels 2–3 cm, massive structure, yellow
	2.4–4.2	Clayey sands, massive structure, yellow-brown
6E	0.0–1.0	Clayey silts, massive structure, yellow
	1.0–1.5	Varied-grain sands, massive structure, yellow
	1.5–2.1	Fine-grained sands, massive structure, light brown
	2.1–2.3	Fine-grained sands, massive structure, yellow
7E	0.0–0.5	Silts, massive structure, light grey
	0.5–1.2	Sandy clays, massive structure, brown-yellow
	1.2–2.2	Medium-grained sands, massive structure, yellow
8E	0.0–0.5	Sandy clays with traces of lamination, yellow
	0.5–1.0	Fine- and medium-grained sands, massive structure, light yellow
	1.0–1.3	Fine-grained, silty sands, streak-laminated with interbeds of silts, grey-brown
	1.3–1.8	Sandy silts and silts, massive structure with traces of organic matter, grey-blue
9E	0.0–0.5	Sandy silts, massive structure, light grey
	0.5–1.5	Clayey sands with interbeds of medium-grained sands, horizontally laminated, grey
	1.5–2.2	Medium-grained sands, massive structure, yellow
10E	0.0–0.5	Silts, massive structure, light grey
	0.5–0.6	Medium- and coarse-grained sands, massive structure, yellow
	0.6–1.1	Clayey sands, brown
	1.1–2.0	Silts, massive structure, light brown
	2.0–2.5	Silty sands, massive structure, light grey
2F	0.0–2.3	Fine-grained sands, massive structure, yellow
4F	0.0–1.3	Sandy silts, massive structure, light grey
	1.3–1.9	Varied-grain sands, massive structure, yellow
	1.9–2.3	Silts and clays with fine-grained sands layers, horizontally laminated, grey-brown
7F	0.0–0.9	Silts, massive structure, light brown
	0.9–1.2	Sandy silts, light brown
	1.2–1.4	Fine-grained sands, yellow
	1.4–2.4	Medium- and fine-grained sands, yellow
9F	0.0–1.0	Sandy silts, massive structure, brown
	1.0–1.5	Varied-grain sands with silts interbeds, horizontally laminated, brown
	1.5–2.2	Fine-grained sands, massive structure, light yellow
11F	0.0–1.5	Fine-grained sands, slightly silty, massive structure, light yellow
	1.5–2.0	Clayey sands with sands interbeds, yellow
	2.0–2.05	Fine gravels, massive structure, yellow
	2.05–2.2	Varied-grain sands, massive structure, yellow
13F	0.0–0.8	Fine-grained, silty sands, massive structure, yellow
	0.8–1.0	Fine-grained sands, massive structure, yellow
	1.0–1.9	Clayey sands, massive structure, grey and yellow at the base
	1.9–2.7	Silty sands, clayey sands, horizontally laminated, yellow
	2.7–2.9	Clayey silts, massive structure, light grey
	2.9–3.0	Medium-grained sands, massive structure, light grey
	3.0–3.2	Clayey silts, massive structure, grey
	3.2–3.3	Medium-grained sands, massive structure, light yellow
14F	0.0–0.9	Clayey sands, massive structure, brown
	0.9–1.0	Fine-grained sands, massive structure, white
	1.0–1.4	Clayey sands, streak-laminated
	1.4–2.1	Varied-grain sands, massive structure, light yellow
	2.1–2.3	Fine-grained sands, massive structure, light yellow
15F	0.0–0.5	Silts, massive structure, grey
	0.5–1.1	Fine-grained, silty sands, massive structure, yellow
	1.1–1.6	Silts, massive structure, yellow-brown
	1.6–1.7	Varied-grain sands with single gravels, massive structure, light yellow
	1.7–2.5	Silts, slightly laminated, yellow
16F	0.0–1.5	Fine-grained sands, massive structure, yellow
	1.5–2.5	Fine-grained sands, horizontally stratification, yellow
18F	0.0–1.5	Silst, massive structure, light brown
	1.5–1.8	Calcareous silts with marl pebbles, light brown
	1.8–2.1	Fine- to medium-grained sands, massive structure, yellow
19F	0.0–1.1	Silts, massive structure, light yellow
	1.1–1.5	Sands with small gravels, massive structure, light yellow
	1.5–1.6	Sandy silts, massive structure, light brown
	1.6–2.2	Silts, massive structure, with sandy silts at the base, brown
	2.2–2.3	Silty sands, massive structure, brown
21F	0.0–1.6	Silts, massive structure, grey
	1.6–2.1	Fine sands with rare gravels, yellow
	2.1–2.3	Silty sands, grey
	2.3–2.5	Fine-grained sands, brown
	2.5–2.7	Sandy silts, flaser lamination, brown
	2.7–3.0	Sandy silts, brownish grey
22F	0.0–1.5	Silts, massive structure, light yellow
	1.5–1.7	Fine-grained sands, massive structure, yellow
	1.7–2.2	Silts, brown, with dispersed organic matter
23F	0.0–1.1	Silts, massive structure, light yellow
	1.1–1.4	Silty sands, horizontal lamination, yellow
	1.4–1.9	Sandy silts, flaser lamination, yellow
	1.9–2.5	Silts, massive structure, light-yellow
	2.5–3.0	Silts, flaser lamination, with dispersed organic matter, dark grey
	3.0–3.9	Silts, humus silts, horizontal lamination, dark grey
24F	0.0-0.7	Silts, massive structure, yellow
	0.7–1.8	Fine-grained sands, massive structure, brown
	1.8–2.1	Silts, massive structure, black
	2.1–3.0	Silty sands, massive structure, grey-black
	3.0–3.2	Medium-grained sands, white
25F	0.0–0.4	Silts, massive structure, yellow
	0.4–0.7	Medium-grained silty sands, massive structure, light brown
	0.7–1.1	Medium-grained sands, yellow
	1.1–1.5	Sandy silts, brown
	1.5–2.2	Sandy silts, single grains of $CaCO_3$, light grey
	2.2–3.1	Fine-grained sands and medium-grained sands, with dispersed organic matter
27F	0.0–1.7	Silts, massive structure, with $CaCO_3$ crumbs at the bottom, yellow
	1.7–2.2	Silty sands, yellow
	2.2–2.5	Sands with rare gravels, light brown
	2.5–3.1	Silts, horizontal lamination, with dispersed organic matter
	3.1–3.3	Silty sands, grey
1I	0.0–0.5	Medium-grained sands, massive structure, yellow
	0.5–1.5	Fine-grained sands, massive structure, light yellow
	1.5–1.9	Fine-grained sands with small gravels, massive structure, yellow
	1.9–2.2	Silts, massive structure, light grey
3I	0.0–1.2	Silty sands with single gravels, massive structure, yellow
	1.2–1.6	Fine-grained sands, massive structure, white
	1.6–2.0	Clayey sands, fine-grained sands, massive structure, light brown
4K	0.0–1.2	Fine-grained silty sands, massive structure, light brown
	1.2–2.4	Fine-grained sands with single gravels, massive structure, light brown
	2.4–2.6	Sandy silts, massive structure, grey
5K	0.0–0.7	Medium-grained sands, massive structure, light yellow
	0.7–3.5	Varied-grain sands, horizontally stratification, light yellow
6U	0.0–1.0	Silty sands, light brown
	1.0–1.6	Medium-grained sands, light brown, with brown clayey inserts
	1.6–2.1	Clays with crystalline gravels, grey-brown
8U	0.0–2.1	Clays with crystalline gravels, grey
	2.1–3.0	Clays with crystalline gravels and chalk fragments, grey
10U	0.0–0.7	Fine-grained sands with gravels, light brown
	0.7–1.2	Clays with interbedding of medium-grained sands, brown
	1.2–1.9	Silty sands, brown
	1.9–2.2	Clays with crystalline gravels, brown
12U	0.0–1.1	Silts, massive structure, light grey
	1.1–1.2	Varied-grain sands, yellow
	1.2–2.2	Sandy silts, massive structure, light grey
	2.2–2.3	Sandy silts with chalk pebbles, massive structure, light grey
15U	0.0–0.6	Sandy silts, massive structure, light brown
	0.6–0.7	Medium-grained silty sands, massive structure, light brown
	0.7–1.0	Medium-grained sands, yellow
	1.0–1.5	Clayey sands/sandy clays, massive structure, light brown
	1.5–2.7	Silts, massive structure, light grey
	2.7–3.5	Medium-grained sands, with organic substance traces at the top, massive structure, light grey
	3.5–3.8	Fine-grained sands, massive structure, yellow
	3.8–3.9	Fine-grained sands, silty, massive structure, yellow
	3.9–4.2	Fine-grained sands, massive structure, yellow
18U	0.0–0.7	Fine-grained sands, massive structure, light brown
	0.7–1.1	Medium-grained sands, massive structure, light brown
	1.1–2.3	Varied-grain sands, silty, massive structure, light brown
19U	0.0–1.0	Varied-grain sands with small gravels, massive structure, yellow
	1.0–2.0	Sands with gravels, massive structure
	2.0–3.2	Varied-grain sands, massive structure, with interlayers of grey silts

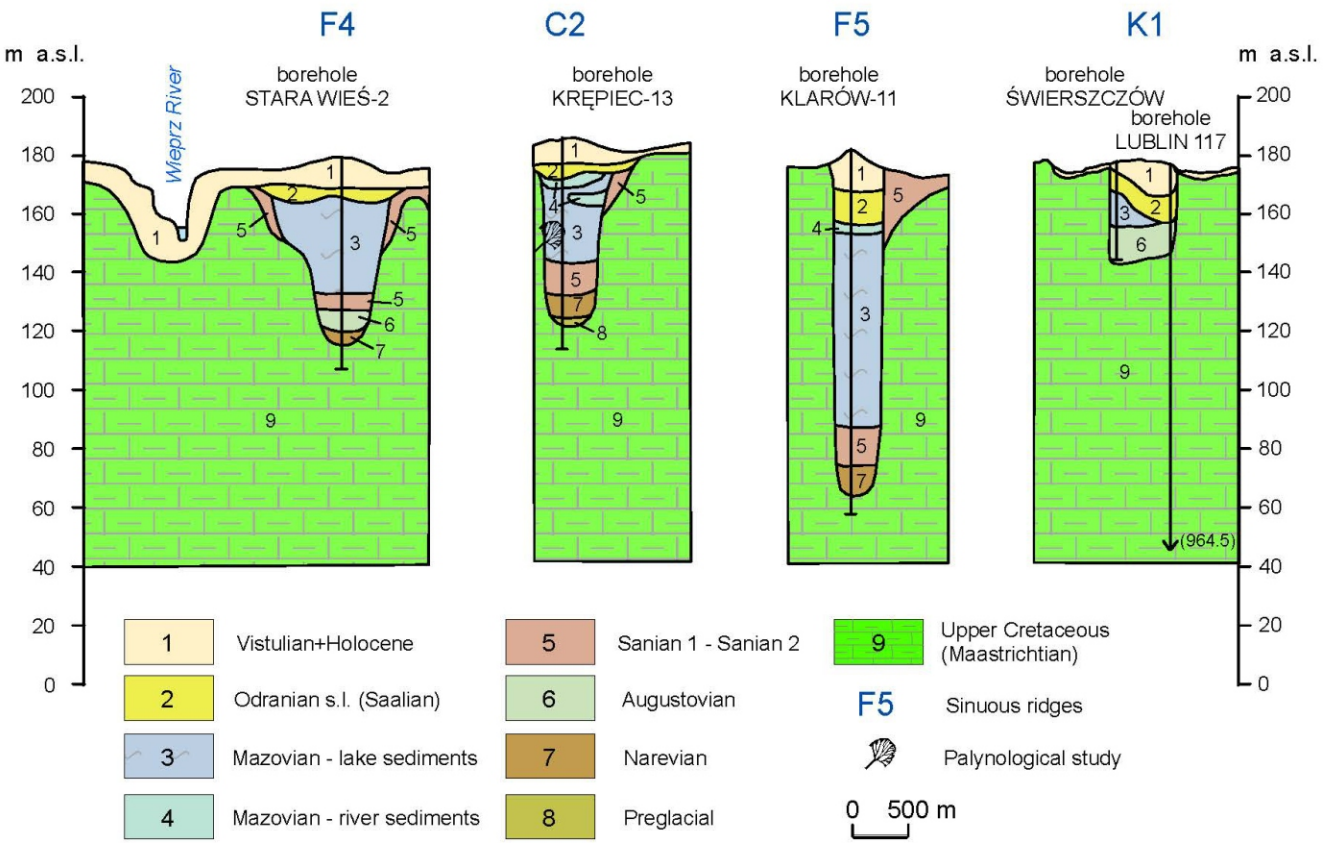

Fig. 7. Inferred glacial trough cross-sections based on archival borehole profiles

Important factor influencing swelling are the hydrogeological conditions and water chemistry. We assume that it is highly likely that the water was enriched in calcium and carbonate ions due to the surrounding rocks, the content of which could have been an additional factor contributing to swelling.

The sub-Quaternary bedrock in the study area also exhibits swelling and shrinkage properties. These rocks are highly porous and rich in calcium carbonate ($CaCO_3$) and are also characterised by high water absorption (Pinińska and Dziedzic, 2006). In addition, the increase in moisture is favoured by the silica they contain. This is a highly hygroscopic compound, i.e. it absorbs and binds water in its structure. The presence of silica causes increased absorption of water molecules by the rock, while during drying, this causes water to be partially retained inside the rock matrix through hydration.

The chalk and Paleogene rocks found in the study area are characterised by high calcium carbonate contents. Opoka rocks are the most resistant of all rock types found here. They contain on average ~62% $CaCO_3$ and SiO_2 in the range of 22 to 37% (Harasimiuk, 1975). An important factor in terms of rock strength is the free silica (opal) content which, together with sponge spicules, forms the rock skeleton. Opoka rocks contain 5–9% free silica (Kowalski, 1961). They are also characterised by high porosity, ranging from 40 to 45% (Harasimiuk, 1975). Limestones studied east of the study area have similar porosity; in the eastern part of the Lublin Upland, they amount to 45% (Bobrowska et al., 2022) and are higher than the average porosity value for limestones, which is 39%. It is estimated that the average porosity of the Upper Cretaceous rocks is very high, ranging from 30 to 50% (Dobrowolski, 2006).

Marl opokas are very similar to opokas in terms of composition and physical properties. They contain slightly more calcium carbonate (~67%) and less silica (~24%; Harasimiuk, 1975). Marls are characterised by an even higher calcium carbonate content (66–73%) and a lower silica content (19–26%; Harasimiuk, 1975).

Chalk has significantly different properties, characterised by a high calcium carbonate content of over 90% and a relatively high silica content (5–6%) as well as a low degree of diagenesis (Harasimiuk, 1975), which makes it a very soft rock. Its compressive strength is low, and it may disintegrate when wet (Kowalski, 1961).

Studies of rock samples from the Chełmskie Hills area (Fig. 2) showed that marls have the highest water absorption by weight, while chalk has the lowest: in marls, the results were 25.16–28.98%, in opokas 20.52–27.10%, in marly opokas 20.92–25.95%, and in chalk 13.45–18.89% (Harasimiuk, 1975). The samples analysed showed an increase in volume during water saturation; the highest was in chalk, which reached 9%, while in marls it was 4–5% (Harasimiuk, 1975).

The strength parameters of the chalk rocks vary but are generally not high. They are lowest for chalk and highest for opoka and gaize. Samples from the Chełm Hills, tested in air-dry conditions, showed a strength not exceeding 5.9 MPa for chalk, and for opoka from 10.7 to 16.7 MPa, and locally up to 19.6 MPa (Harasimiuk, 1975). Studies of Miocene limestones from the eastern Lublin Upland showed compressive strength ranging from 9 MPa to 16 MPa (average 13 Mpa; Bobrowska et al., 2022). The resistance of samples to uniaxial compression decreases gradually with increasing water content, while in a

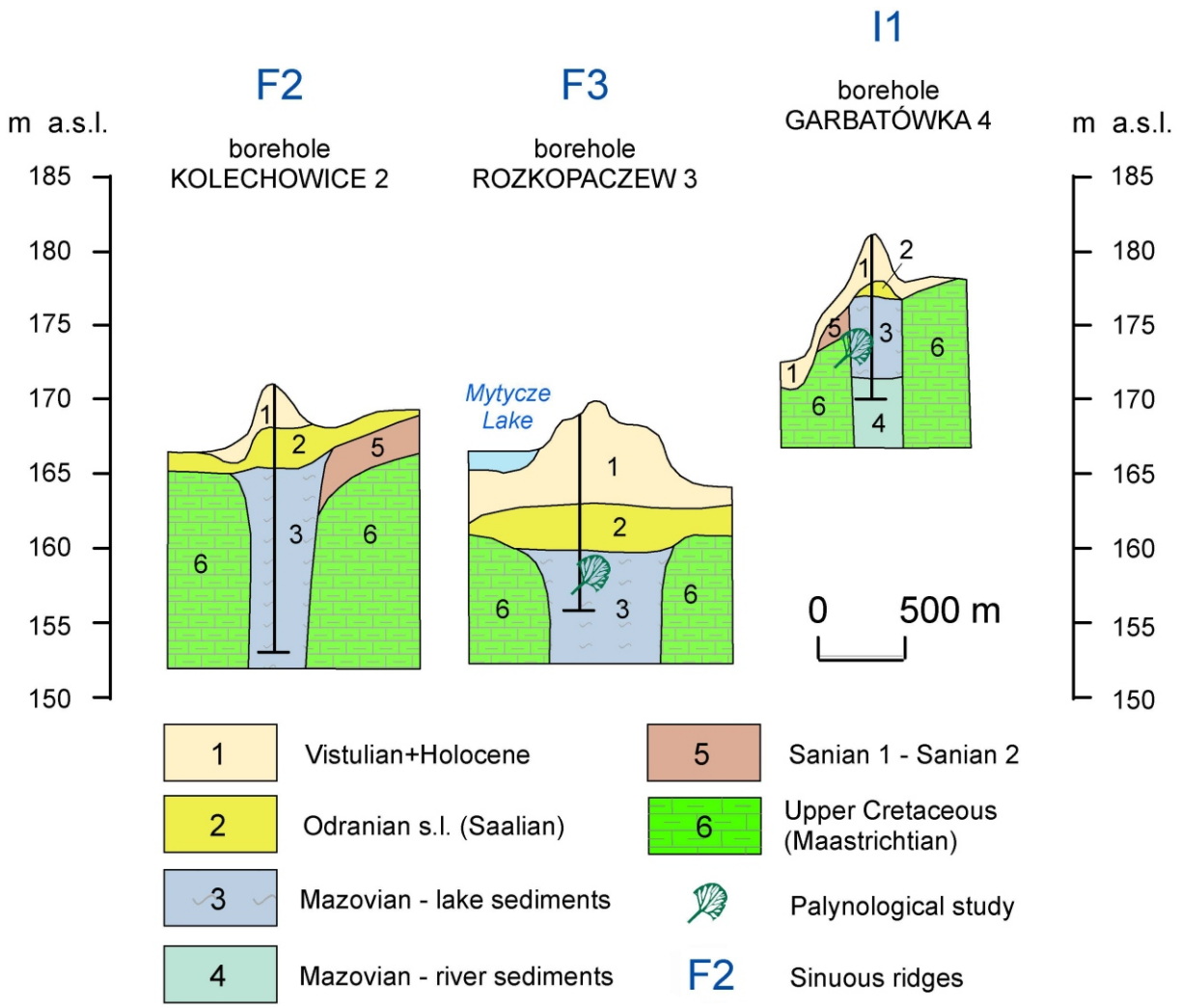

Fig. 8. Glacial trough diagrams based on new boreholes made for this study

frozen state, the compression test proved impossible due to the dissolution and destruction of rock samples (Bobrowska et al., 2022).

At the current stage of research, no laboratory analyses of the swelling susceptibility of rocks occurring in the study area have been carried out, nor have detailed mineral composition studies of the deposits been made. The influence of this factor was considered only theoretically, based on available geological borehole profiles (Fig. 3) and archival materials (e.g., Liszkowski, 1979a, b; Harasimiuk and Henkiel, 1980a, b, Krawczyk, 2023a, b; Krawczyk and Kucharska, 2023a, b; Buraczyński and Wojtanowicz, 1981a, b; Kucharska, 2023a, b).

Further research will focus on determining the mechanical properties of the carbonate rocks, as well as on the content of clay mineral and $CaCO_3$ contents of the clastic deposits.

DISCUSSION

Our research has documented a number of sinuous ridge forms. Sinuous ridges in the study area can have various origins. The first group consists of postglacial forms created within the ice sheet, such as fissures, eskers and kames. The second group consists of the inverted channels we have studied.

In previous studies, sinuous ridges occurring in Polesie were considered mainly as postglacial forms or comprising fluvioperiglacial deposits forming distinct geological structures (e.g., Liszkowski, 1979a, b; Stochlak, 1979a, b; Buraczyński and Wojtanowicz, 1981a, b, 1982a, b, 1987a, b; Harasimiuk et al, 2017; Żarski and Tekielska, 2023; Fig. 1). Many smaller or less distinct forms were not included in the studies as separate landforms (Liszkowski, 1979b; Harasimiuk and Henkiel, 1980b; Buraczyński and Wojtanowicz, 1981b, 1987b; Butrym et al., 1982; Harasimiuk et al., 2017; Fig. 1).

Our detailed DTM analysis, fieldwork and research identified the sinuous ridges in the study area and showed that they belong to two genetic types: glacial forms and inverted channels. The forms characterised by inverted channels are the only forms of this type found in Poland to date. We rule out their glacial origin, and provide an interpretation for their formation.

Based on field studies and geophysical surveys, it was concluded that forms W3 and Y1 show characteristics of post-glacial forms. The data indicate that the geological structure of the ridge, together with the deposits at its base forming the trough fill, are integral. This suggests that the entire structure was formed during a single-stage process. This interpretation was corroborated by geophysical surveys (Fig. 6).

Examination of the ridges from sequences E, F, I and K revealed that they show characteristics of inverted channels and are not glacial forms, as indicated by a number of documented features. Despite their morphometric similarities to glacial forms, certain distinctive features can be observed in their structure. The ridges are clearly flat-topped. Forms F create a distinct system stretching for many kilometres, resembling a

gently meandering river valley. Analysis of the profiles of shallow boreholes drilled within these forms reveals a pattern (Table 4). The upper part comprises lithologies deposited in low-energy flowing waters or in standing waters: silty sands and silty clays (SFm), sandy silts (FSm) and silts (Fm) with a massive structure. Below these, there is usually a succession of sandy deposits reflecting fluvial sedimentation: fine- and medium-grained winnowed sands, in which horizontal layering (Sh) and thin interlayers of clays (F), silts (F) and sandy silts (FS) can locally be observed, indicating variable flow dynamics. Locally, fine gravel (G) occurs as an admixture in these deposits. Below the sands, reservoir sediments such as horizontally layered silt and silty sand (Fh) are found. In the profiles of some boreholes, interlayers with organic matter occur. Despite the positive topographic form, the deposits show characteristics of lacustrine sediments with periodic inflows. In the north-western part of the study area, Liszkowski (1979a) found evidence of southwards sedimentary transport in several exposures. The deposits forming the morphological ridge maintain sedimentary continuity with the deposits underlying a given form. There is no clear boundary in the sedimentary profile at the morphological boundary of the ridge. The deposits occurring above and below the level of the base of the ridge represent a record of continuous sedimentation in a water body.

The glacial origin of the forms analysed was ruled out by the numerical age dating of the sedimentary deposits forming the ridges. In one sample, the result indicated that sedimentation ended in the early Holocene; in 11 samples, the dating indicated that sedimentation continued into the late Vistulian (late glacial), and in 3 samples, the dating indicated sedimentation in the Odranian (Saalian) or Mazovian (Holsteinian). The sampling depth was ~1.5 m, which suggests the possibility of the existence of forms younger than those indicated by the dates obtained.

The second important evidence for the non-glacial nature of the sinuous ridges is provided by palaeogeographic and palynostratigraphic studies, which are based on recently established views showing that the last ice sheet to completely cover the study area was the Sanian 2 (Elsterian) ice sheet (e.g., Marks et al., 2018; Hrynowiecka et al., 2019; Żarski and Kucharska, 2020; Marks, 2023; Żarski et al., 2024). By studying the biogenic deposits found under the sinuous ridges, it was possible to constrain their origin.

The biogenic deposits were dated using samples obtained from erosional incisions located under sinuous ridge forms. We interpet these incisions as subglacial troughs. They are filled with secondary deposits of various origins and ages (clay, sand, silt and peat), which also excludes a fissure origin for these forms. We have documented Mazovian (Holsteinian) interglacial deposits the Rozkopaczew 3 borehole on ridge F3 and Garbatówka 4 borehole (Krawczyk, 2023a; Kucharska, 2023a) on ridge I1, as well as in the Krępiec-13 borehole on ridge C2 (Janczyk-Kopikowa, 1981), while lake deposits interpreted as of the Mazovian interglacial were found in the Klarów-11 borehole (Harasimiuk and Henkiel, 1980a, b) on ridge F5, located in depressions beneath the sinuous ridges, indicate a younger age of the forms than that of the interglacial. Above the lake succession studied, there are deposits that do not show glacial characteristics. Since no ice sheet occupied the study area after the Mazovian interglacial, the glacial origin of some sinuous ridge forms, as suggested by SMGP authors (e.g., Liszkowski, 1979a, b; Stochlak, 1979a, b; Buraczyński and Wojtanowicz, 1981a, b, 1982a, b, 1987a, b; Harasimiuk et al, 2017), should be excluded.

The areas adjacent to the ridges are composed of deposits similar to or more resistant to erosion than the ridges themselves. The possibility of relief inversion caused by chemical denudation of chalk rocks in the vicinity of the forms was considered. Chemical denudation of adjacent areas could not have caused a levelling of 3–8 m, as this is the height of the forms described, since the average rate of chemical denudation of carbonate rocks in this area is 10–22 mm/100 years (Świeca, 2000; Maruszczak, 2001), which gives ~50 cm over the last 20,000 years.

Excluding a glacial origin for the sinuous ridges E, F, I, K, and presumably C2 and others, and excuding chemical denudation, we interpret them as inverted channels and below seek to determine the origin in terms of this process. The starting point was the experience of scientists studying similar forms around the world. It is known that the form of inverted channels depends on two main factors. The first is the cementation of sedimentary deposits filling a previously formed channel. The second process, following the first, is the exhumation of the channel-fill, which leads to the final formation of the inverted channels.

The factors causing the formation of inverted channels as described by, e.g., Zaki et al. (2021), namely cementation and exhumation of the cemented deposits, cannot be transposed to the forms found in Polesie. The ridges under study are composed of fine-grained, loose, uncemented and unsilicified deposits, which are not resistant to weathering, whether by water or wind erosion. OSL dating indicate their young age and sedimentation at the end of the Vistulian. The preservation and palaeogeography of the area also indicate that these are young forms and deposits. Morphometric and DTM analyses show the distinctiveness of these forms and the absence of extensive denudation. Factors contributing to the formation of inverted palaeochannels, such as volcanism (e.g., Cundari and Ollier, 1970; Biek et al., 2000; Sias, 2002), tectonics (e.g., Parry, 1996; Hill et al., 2003) or the burning or deflation of adjacent organic deposits (Ellery et al., 1989; Gumbricht et al., 2004; Smith et al., 2010), should be excluded. Sedimentary cementation and armouring should also be excluded (e.g., Parry, 1996; Marchetti et al., 2005; Williams et al., 2021), as the Polesie forms do not have a cover of resistant 'armour', and are not cemented.

As shown by the above analysis of various views on the formation of sinuous ridges and their specific variety, inverted channels, none of them can be directly applied to explain the formation of these forms in Polesie. We conclude that the forms discussed here (in particular the more thoroughly investigated forms C2, D1, E, F, I and K) were created with the participation of water and can be interpreted as inverted fluvial channels. Such forms can also be described as a specific type of signature of an aqueous landform.

Below we provide a hypothesis explaining how these inverted fluvial channels were formed in Polesie.

We consider that deeply cut subglacial troughs played a very important role in the formation of the ridges, their creation being linked to pre-Mazovian glaciations. Most likely, the troughs were formed during the South Polish glaciations, and perhaps even earlier, during the Narevian glaciation, as indicated by the presence of glacial clays from that interval in some troughs (Lisicki, 2003; Kucharska et al., 2024; Fig. 9A).

Subglacial troughs, formed during glaciation, were incorporated into the local hydrographic network and subsequently functioned as fluvioglacial drainage routes and as river valleys and lakes (Fig. 9A; Kucharska et al., 2024). Within the troughs, erosional and sedimentary processes alternated. After the re-

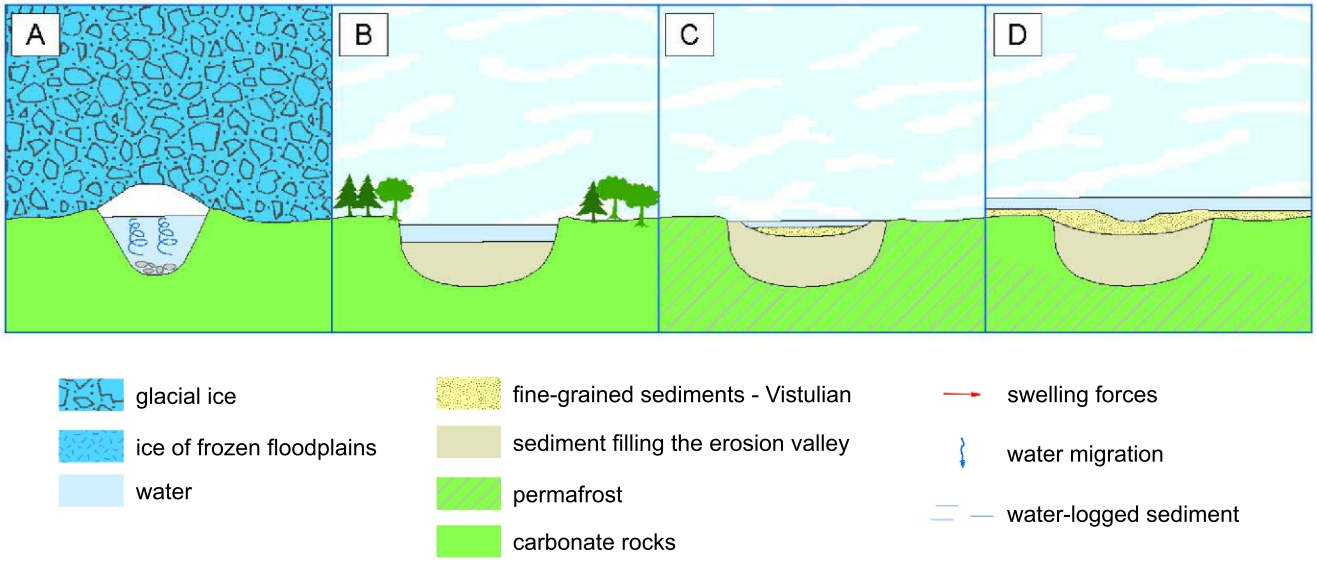

Fig. 9. Diagram of erosional trough formation and subsequent infill

A – pre-Mazovian interglacial interval. Formation of subglacial troughs. Glacial erosion and glacial and fluvial sedimentation; **B** – interglacial periods. Functioning of erosion troughs as river valleys and lakes. Deposition of river and lake sediments; **C** – Vistulian. Period of periglacial conditions. Formation of permafrost, periodic activation of flows along old valley routes; **D** – Late Glacial, Bølling/Allerød. Formation of extensive floodplains, deposition of fine-grained sediments

treat of the last ice sheet, Sanian 2 (Elsterian), sedimentation began to dominate. The valley depressions were gradually infilled (Fig. 9B). Lacustrine sedimentation dominated, as shown by the fine-grained trough infill, such as fine-grained sands, silts and clays, and organic deposits. Lacustrine sedimentation continued in both interglacial and periglacial conditions. Most likely, these lakes were of a flow-through nature, as indicated by fluvial interlayers in the lake deposits (Kucharska et al., 2024).

During the periglacial conditions of the Vistulian, permafrost formed again (Fig. 9C). During warming periods, flow was periodically activated, using the former waterways. Fine-grained sediments continued to be deposited in the old valleys. As indicated by the OSL dates obtained, sedimentation of ridge sediments continued throughout the Vistulian and the beginning of the Holocene (from ~91.0 to ~7.0 kyr BP). However, the concentration of age results within the range of 12–19 kyr clearly indicates increased sedimentation in the late glacial period. Therefore, it can be assumed that the final formation of the ridges must have taken place at the end of the Vistulian or at the transition from the Vistulian to the Holocene.

In the Vistulian and at the beginning of the Holocene, warming became rapid, particularly between 14.3 and 12.8 ka BP, which is identified with the Bølling/Allerød interval, and then between 11.5 and 8.8 ka BP, i.e. after the Younger Dryas (Stanford et al., 2010). These warmings caused rapid melting of ice sheets and a sharp rise in global sea levels, which at their peak could reach 250 cm/100 years (Lambeck et al., 2002; Stanford et al., 2010). In the study area, higher river terrace deposits and Vistulian mud covers occur at altitudes of 170–185 m a.s.l., while present-day water levels in the valleys are at altitudes of 155–165 m a.s.l. This indicates that, during the Vistulian, the valleys were located at significantly higher elevations than today. In the Chełm Hills area during this interval, under periglacial climate conditions on extensive lake-type floodplains, the accumulation of sandy-silty deposits reached an altitude of 190–195 m a.s.l. (Harasimiuk, 1975). The rapid release of water stored in ice sheets caused a very rapid rise in water levels in areas close to melting ice sheets. This was facilitated by extensive depressions, such as basins and troughs, which, with permafrost forming an impermeable layer, became traps for the released water. Extensive floodplains were formed in these areas, including in the study area. At the same time, erosional processes began, and previously accumulated sediments were transported to depressions.

During the Bølling/Allerød (Fig. 9D), an extensive floodplain formed in the study area. This is shown by the extensive fine-grained, thin-bedded Vistulian lake-river (floodplain) deposits found at the surface (Harasimiuk et al., 2004; Krawczyk, 2023a, b; Kucharska, 2023a, b, 2025a, b; Krawczyk and Kucharska, 2023a, b). During the brief Alleröd warming period, the average annual temperature in this region may have increased by as much as 4.7°C, (Maruszczak, 1974a, b; Dobrowolski, 2006).

At the end of the Vistulian, there must have been a confluence of various factors that caused the formation of such specific forms as those in the study area of Polesie, with a different structure from those known and described in the literature. They can be divided into two main groups.

THE FIRST GROUP OF FACTORS CAUSING THE FORMATION OF THE INVERTED FLUVIAL CHANNELS

The cooling during the Younger Dryas caused the floodplains to freeze and form an extensive ice cover. Despite the formation of the ice cover, water flow did not cease completely, but continued in the former river valleys, locally beneath the ice surface (Fig. 10A). Their dynamics were clearly weakened compared to those of ice-free conditions. River cross-section flow decreased, and ice jams and flow blockages could form, which favoured increased sedimentation. These factors caused the channels carved in the ice covers to fill with fine-grained sediments. It cannot be ruled out that sedimentation occurred when the river surfaces were frozen and flow took

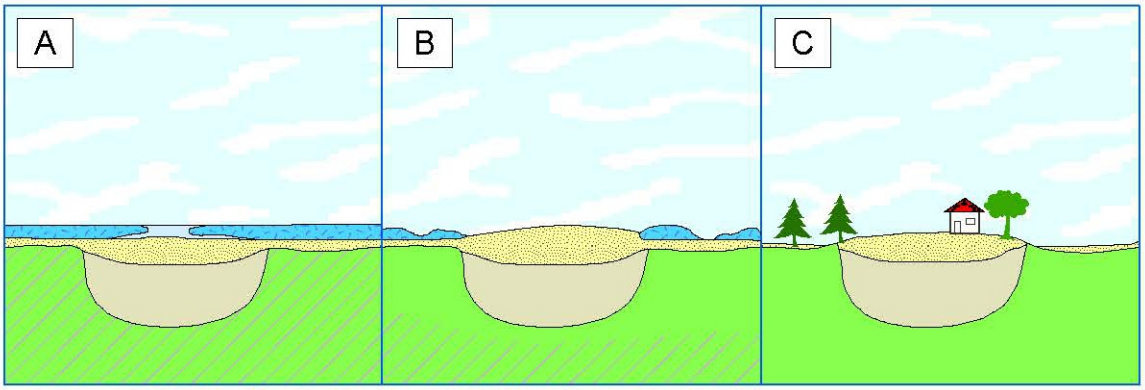

Fig. 10. Diagram of inverted fluvial channel formation – first group of factors (explanations as for Fig. 9)

A – Younger Dryas. Cooling, freezing of floodplains, formation of floodplain ice covers, concentration of flows in former river channels, slow decline of flow, increased sedimentation, filling of ice troughs with sediments; **B** – end of the Vistulian. Thawing of floodplains, disappearance of permafrost; **C** – Holocene. Thawing of floodplains, disappearance of permafrost, formation of inverted fluvial channels from deposits accumulated in ice troughs

place under the ice. A mechanism similar to the formation of englacial eskers occurred, except that it involved river water and floodplain ice.

The sedimentation of ridge deposits ended mainly in the Younger Dryas, i.e. 12.65–11.55 ka BP (Fig. 10B). Ice troughs and, locally, ice tunnels were filled with fine-grained sediments, which constricted the flows until they stopped completely.

Another rapid warming (pre-Boreal) between ~11.5 and 9.0 ka BP (Lambeck et al., 2002; Stanford et al., 2010) caused the final melting of the Vistulian ice sheet, unblocking the northward flow of water, and in the study area, the melting of floodplain ice and the disappearance of permafrost (Dobrowolski, 2006). The deposits accumulated in ice troughs formed positive topographic features – inverted fluvial channels (Fig. 10C), causing a change in the river network in the study area.

THE SECOND GROUP OF FACTORS CAUSING THE FORMATION OF INVERTED FLUVIAL CHANNELS

The second theory that may explain the formation of the sinuous ridges as inverted fluvial channels is related to rock parameters such as swelling and shrinkage. The deposits filling the troughs are predominantly fine-grained, which are very susceptible to swelling and associated expansion. The carbonate rocks of the Maastrichtian surrounding the troughs also have specific swelling properties.

The Bølling/Allerød warming, in addition to its association with the formation of extensive floodplains, also caused the partial disappearance of permafrost and an increase in the active layer, but not its complete disappearance (Dobrowolski, 2006).

The lowering of the impermeable layer, which was the permafrost zone, resulted in the unblocking of fissures through which water penetrated deep into the rock mass (Dobrowolski, 2006). In the Younger Dryas there was a temporary slowing down of these processes. Water infiltration was also favoured by the vicinity of subglacial troughs. The rocks of the Middle Cretaceous: chalk, marls and opoka received and stored large quantities of water, which could not drain into the rock mass. The specific properties of the Upper Cretaceous rocks of the study area meant that, despite their high porosity and fracturing, these rocks have a low filtration coefficient of 10^{-7}–10^{-11} m/s (Dobrowolski, 2006). Therefore, these rocks are considered to be almost impermeable and there is very little underground drainage of water. It is assumed that the zone of infiltration reaches up to 100 m at most in the chalk and marls and 150 m in the opoka, and water infiltrates only at the contact of fault zones (Dobrowolski, 2006). Under these conditions, the waters occurring in the Cretaceous rocks may have been tied up in the near-surface zone, reaching from a few tens to ~100 m.

Large quantities of water caused a change in the rock structure, followed by swelling (Fig. 11A). The walls of the deep and relatively narrow troughs, extending over many kilometres, were deformed and gradually narrowed. The fine-grained clastic (silty-plastic) deposits, which constitute the trough infills, were also very susceptible to swelling. They, too, became very heavily saturated with water at this time, causing them to swell and become more plastic. The more plastic-prone deposits filling the troughs were gradually pushed upwards. Along the troughs an inversion of relief occurred, sinuous ridges were formed, which are the inverted fluvial channels (Fig. 11B). After the disappearance of the permafrost, there was a partial drainage of water into the rock mass, as well as drying of the area, due to the lowering of the water level. The specific parameters of the carbonate rocks meant that they no longer returned to their previous position (Fig. 11C). This process was strongly influenced by the presence of silica, which, as noted earlier, together with the sponge spicules, forms the rock skeleton; this, after drying, caused an increase in their strength.

Both of the groups of factors described relate to the final formation of ridges in the study area, and their common driver is climate change, which caused fluctuations in water levels and significant temperature changes.

We believe that the forms occurring in Polesie arose as a result of the interaction of the both groups of factors presented, with their intensity varying over time. The genesis suggested in the first diagram (Fig. 10) does not seem sufficient to explain the formation of these forms, since their occurrence has not been recorded in other regions of Poland, where similar climatic conditions prevailed at the end of the last glaciation.

In the case of the study area, the geological structure was of key importance. One of the characteristics of the study area is the presence of carbonate rocks in the sub-Quaternary bedrock, mainly marls, opoka and chalk. Overlying these is a relatively thin layer of Pleistocene deposits. Deep subglacial troughs, now filled with fine-grained clastic deposits, were incised in the carbonate rocks. These conditions may have promoted the formation of the alternative genesis shown in the second diagram (Fig. 11), related to the lithological properties of the substrate.

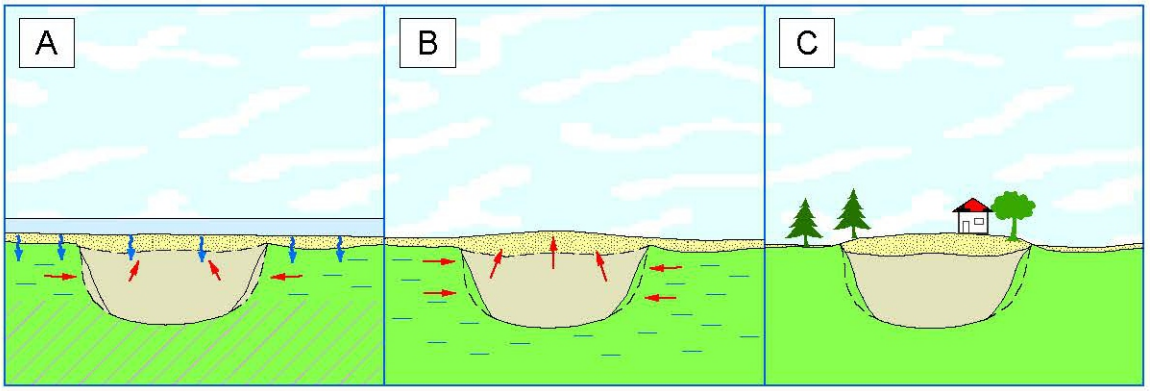

Fig. 11. Diagram of inverted fluvial channel formation – second group of factors (explanations as for Fig. 9)

A – Bølling/Allerød. Partial disappearance of permafrost. Strong water infiltration into the rock mass. Initiation of swelling and upward extrusion of trough deposits; **B** – pre-Boreal period. Lowering of the impermeable permafrost layer until complete disappearance. Strong water infiltration into the rock mass. Pushing of sediments upwards, formation of inverted fluvial channels; **C** – Holocene. Final formation of sinuous ridges

The joint interaction of the two groups of factors created conditions conducive to the formation of sinuous ridges. We cannot determine unequivocally which process played the dominant role. However, it is known that their intensity fluctuated at different times during the transition from the Vistulian to the Holocene.

In the first group of factors, the sedimentation factor was indicated as the causative factor. In this hypothesis, the most important issue is the melting of the spillway ice and the development of channelized flow, which allowed the deposition of sandy sediments, which then, after the ice melted, assumed a topographically positive form. Sedimentation took place in the late Dryas, at a time when much of the water was trapped on the frozen floodplains.

In the second group of factors, the most important role was played by the mechanical parameters of the rocks. From the time of the Bølling/Allerød warming, until the beginning of the Holocene, there were rapid climatic changes causing the release of large masses of water and the disappearance of permafrost. Infiltration of water deep into the rock mass had a major impact on changes in the mechanical parameters of the bedrock and Quaternary deposits filling the subglacial troughs. Swelling of the carbonate rocks of the sub-Quaternary rock mass was triggered, which caused the subglacial troughs to narrow. The fine-grained deposits in the troughs, due to the large amount of water, became more plastic, swelled and, together with the deposits accumulated in the ice troughs, pushed upwards.

he survey material described was collected as part of mapping work for the SMGP rather than towards investigating the structure and genesis of the ridge. There are many aspects to be further clarified, such as the geological structure of the U4 ridge, where glacial clays have been documented at the surface, which may corroborate the 2nd swelling theory or indicate that the entire U4 structure has a post-glacial genesis. A further phase of work is planned to carry out sedimentological studies of the deposits building the ridge and its vicinity. The geotechnical parameters of the rocks building the subsoil in the area of the ridges and the deposits filling the troughs beneath the ridges also need analysis. Analyses and simulations of sedimentary behaviour under the influence of permafrost and high humidity, especially swelling and shrinkage, are planned.

CONCLUSIONS

We document the occurrence of many sinuous ridge forms, of two genetic types, in the study area. The first type comprises sinuous ridges, which are post-glacial forms; these include the W3 and Y1 forms. The second type are sinuous ridges interpreted as inverted fluvial channels and include forms C2, D1, I1, K1 and the series of forms E and F. The remaining forms require further detailed study. Forms defined as inverted fluvial channels are so far the only ones of this type in Poland, and probably the only ones recognized in the world, with such an atypical geological structure.

Sinuous ridges, which are post-glacial forms (W3 and Y1) are partly composed of coarse clastic sand and gravel deposits with boulders, indicating high energy sedimentation.

Inverted fluvial channels are specific signatures of water-formed landforms, and the deposits that build them have characteristics typical of river-lake and lake-river sediments. They comprise alternating silty deposits with fine- and medium-grained sands without a silt fraction. There are also organic-rich interbeds within these deposits. There is sedimentary continuity between the deposits building the ridge topography and the sediments below, with no clear sedimentary boundary at the level of the morphological boundary of the ridge.

The dating of the deposits which we consider to be inverted fluvial channels, indicated a young age of sedimentation (Vistulian/Weichselian). Most dates are in the range of 12-19 kyr, putting this time interval in the Late Glacial. The dates obtained of 180–210 kyr BP from the H2, U3 and V1 ridges may indicate temporally extended sedimentation of individual ridge sediments. The older dates, however, do not exclude ridge formations at a later time, during a single episode at the transition of the Vistulian to the Holocene, as the method of sampling only allowed time constraint on material at the sampling level and not above it.

The geophysical survey and geological drilling carried out, as well as the analysis of archival materials, showed that a very important element in the creation of these forms are the depressions occurring beneath them, and in the bedrock in which these depressions were eroded. They have the character of subglacial troughs, formed in chalky sub-Quaternary bedrock, composed of carbonate rocks of the Maastrichtian. The depres-

sions occur beneath inverted fluvial channels and are of considerable depth. The deepest documented depression under the F5 ridge reaches a depth of over 85 m. The trough sedimentary infills are of various ages, with fine-grained clastic deposits such as silts, fine sands and clays predominating.

The documented deposits of the Mazovian interglacial in the troughs clearly exclude a post-glacial genesis for the inverted fluvial channels.

The analyses carried out showed that we have to be very cautious in classifying forms of sinuous ridges as inverted channels, as there are also eskers, kames, crevasses and fluvioglacial forms in the post-glacial area. Without depth profiling analysis of the geological structure and obtaining evidence, such as numerical dates and palynological spectra, it cannot be conclusively established that a form represents an inverted fluvial channel.

The inverted fluvial channels occurring in Polesie were formed as the Vistulian gave way to the Holocene, associated with former subglacial troughs. The main reason for their formation was the rapid climatic changes occurring at the time. Warming in the late Glacial, during the Bölling/Alleröd phase, led to the formation of extensive floodplains, which partially froze during the younger Dryas, forming a wide sheet of floodplain ice. Within it, in places of former river channels, water flow still persisted and did not disappear even beneath the ice cover. Progressive cooling led to a weakening of flow and increased sedimentation. As a result, the river channels became filled with fine-grained sediments.

The next phase of warming, coinciding with the beginning of the Holocene, resulted in the complete melting of the floodplain ice and the transformation of sediment-filled channels into ridges known as inverted fluvial channels. The second group of factors co-responsible for the formation of these structures was the mechanical properties of the rocks. These included the swelling of carbonate bedrock and the swelling and pushing upwards of fine-grained deposits accumulated in former subglacial troughs. These processes together contributed to the formation of the inverted fluvial channels. At the present stage of research, however, it is difficult to determine unequivocally which of these factors played the dominant role in their formation.

Acknowledgements. We would like to thank two reviewers, Professor Sławomir Terpiłowski and Dr. Abdallah S. Zaki, for their valuable comments and suggestions, which contributed to the improvement of our manuscript. We would also like to thank dr Bogusław Przybylski, Chief Coordinator of SMGP in 2018–2024, who was the first to point out the similarity of unusual forms in Polesie to those found in other parts of the world and on Mars. We would like to thank dr Alicja Bobrowska from the Faculty of Geology at the University of Warsaw for her consultations on the mechanical properties of carbonate rocks found in the study area. The study was financially supported by the Polish Geological Institute – National Research Institute research projects: "National tasks performed by the National Geological Survey with regard to geological mapping realized from 2018. Update of the Detailed Geological Map of Poland in the scale 1:50,000" (22.0013.1801.02.1).

REFERENCES

Aref, M.A.M., 2003. Classification and depositional environments of quaternary pedogenic gypsum crusts (gypcrete) from east of the Fayum Depression, Egypt. Sedimentary Geology, **155**: 87–108; https://doi.org/10.1016/S0037-0738(02)00162-8

Bell, R.B., Williamson, I.T., 2013. A Palaeocene intracanyon-style lava emplaced during the early shield-building stage of the Cuillin Volcano, Isle of Skye, NW Scotland. Earth and Environmental Science Transactions of the Royal Society of Edinburgh, **104**: 205–230; https://doi.org/10.1017/S1755691013000509

Beresford-Jones, D.G., Susana, A.T., Whaley, O.Q, Chepstow-Lusty, A.J., 2009. The role of Prosopis in ecological and landscape change in the Samaca Basin, Lower Ica Valley, South Coast Peru from the Early Horizon to the Late Intermediate Period. Latin American Antiquity, **20**: 303–332; https://doi.org/10.1017/S1045663500002650

Biek, R.F., Willis, G.C., Hylland, M.D., Doelling, H.H., 2000. Geology of Zion National Park, Utah. Utah Geological Association Publication, **28**: 106–138; https://www.govinfo.gov/content/pkg/GOVPUB-I29-PURL-gpo79287/pdf/GOVPUB-I29-PURL-gpo79287.pdf

Bobrowska, A., Jagoda, E., Domonik, A., Ryżyński, G., 2022. Thermomechanical properties of detrital limestone from the Nowe Brusno town (Poland). Resources Policy, **77**, 102456; https://doi.org/10.1016/j.resourpol.2022.102698

Bristow, C.S., Drake, N., Armitage, S., 2009. Deflation in the dustiest place on Earth: The Bodélé Depression, Chad. Geomorphology, **105**: 50–58; https://doi.org/10.1016/j.geomorph.2007.12.014

Buraczyński, J., Wojtanowicz, J., 1981a. Objaśnienia do Szczegółowej Mapy Geologicznej Polski w skali 1:50 000. Arkusz Orzechów Nowy (715) (in Polish). CAG, Warszawa; https://bazadata.pgi.gov.pl/data/smgp/arkusze_txt/old/smgp0715old.pdf

Buraczyński, J., Wojtanowicz, J., 1981b. Szczegółowa Mapa Geologiczna Polski w skali 1:50 000. Arkusz Orzechów Nowy (715) (in Polish). CAG, Warszawa; https://bazadata.pgi.gov.pl/data/smgp/arkusze_skany/old/smgp0715old.jpg

Buraczyński, J., Wojtanowicz, J., 1982a. Objaśnienia do Szczegółowej Mapay Geologicznej Polski w skali 1:50 000. Arkusz Kołacze (716) (in Polish). CAG, Warszawa; https://bazadata.pgi.gov.pl/data/smgp/arkusze_txt/old/smgp0716old.pdf

Buraczyński, J., Wojtanowicz, J., 1982b. Szczegółowa Mapa Geologiczna Polski w skali 1:50 000. Arkusz kołacze (716) (in Polish). CAG, Warszawa; https://bazadata.pgi.gov.pl/data/smgp/arkusze_skany/old/smgp0716old.jpg

Buraczyński, J., Wojtanowicz, J., 1987a. Objaśnienia do Szczegółowej Mapy Geologicznej Polski w skali 1:50 000. Arkusz Sawin (752) (in Polish). CAG, Warszawa; https://bazadata.pgi.gov.pl/data/smgp/arkusze_txt/smgp0752.pdf

Buraczyński, J., Wojtanowicz, J., 1987b. Szczegółowa Mapa Geologiczna Polski w skali 1:50 000. Arkusz Sawin (752) (in Polish). CAG, Warszawa; https://bazadata.pgi.gov.pl/data/smgp/arkusze_skany/smgp0752.jpg

Bussert, R., Eisawi, A.A.M., Hamed, B., Babikir, A.A., 2018. Neogene palaeochannel deposits in Sudan – Remnants of a trans-Saharan river system? Journal of African Earth Sciences, **141**: 9–21; https://doi.org/10.1016/j.jafrearsci.2017.11.040

Butrym, J., Harasimiuk, M., Henkiel, A., 1982. Szczegółowa Mapa Geologiczna Polski w skali 1:50 000. Arkusz Lublin (749) (in Polish). CAG, Warszawa; https://bazadata.pgi.gov.pl/data/smgp/arkusze_skany/smgp0749.jpg

Butt, C.R.M., Bristow, A.P.J., 2013. Relief inversion in the geomorphological evolution of sub-Saharan West Africa. Geomorphology, **185**: 16–26; https://doi.org/10.1016/j.geomorph.2012.11.024

Cas, R.A.F., Wright, H.M.N., Folkes C.B., Lesti. Ch, Porreca, M., Giordano, G., Viramonte, J.G., 2011. The flow dynamics of an extremely large volume pyroclastic flow, the 2.08-Ma Cerro Galan Ignimbrite, NW Argentina, and comparison with other flow types. Bulletin of Volcanology, **73**: 1583–1609; https://doi.org/10.1007/s00445-011-0564-y

Clarke, J.D.A., Stoker, C.R., 2011. Concretions in exhumed and inverted channels near Hanksville Utah: implications for Mars. International Journal of Astrobiology, **10**: 161–175; https://doi.org/10.1017/S1473550411000048

Cuevas Martínez, J.L., Pérez, L.C., Marcuello, A., Cazo, P.A., Marzo Carpio, M., Bellmunt, F., 2010. Exhumed channel sandstone networks within fluvial fan deposits from the Oligo-Miocene Caspe Formation, south-east Ebro Basin (north-east Spain). Sedimentology, **57**: 162–189; https://doi.org/10.1111/j.1365-3091.2009.01096.x

Cundari, A., Oilier, C.D., 1970. Australian landform example no. 17; Inverted relief due to lava flows along valleys. Australian Geographer, **11**: 291–293; https://doi.org/10.1080/00049187008702563

Doctor, D.H., Orndorff, W., Maynard, J., Heller, M.J., Casile, G.C., 2014. Karst geomorphology and hydrology of the Shenandoah Valley near Harrisonburg, Virginia. GSA Field Guide, **35**: 161–213; https://doi.org/10.1130/2014.0035(06)

Dobrowolski, R., 2006. Glacial and periglacial transformation of karst relief in the northern foreland of the Lublin-Volhynia uplands (SE Poland, NW Ukraine) (in Polish with English summary). Wydaw. UMCS, Lublin.

Ellery, W.N., Ellery, K., McCarthy, T.S., Cairncross, B., Oelofse, R., 1989. A peat fire in the Okavango Delta, Botswana, and its importance as an ecosystem process. African Journal of Ecology, **27**: 7–21; https://doi.org/10.1111/j.1365-2028.1989.tb00924.x

Foix, N., Allard, J.O., Paredes, J.M., Giacosa, R.E., 2012. Fluvial styles, palaeohydrology and modern analogues of an exhumed, Cretaceous fluvial system: Cerro Barcino Formation, Cañadón Asfalto Basin, Argentina. Cretaceous Research, **34**: 298–307; https://doi.org/10.1016/j.cretres.2011.11.010

Foix, N., Allard, J.O., Ocampo, S.M., Paredes, J.M. 2018. Afloramientos tridimensionales de paleocanales exhumados (Grupo Chubut, Cuenca de Cañadón Asfalto) como análogos de reservorios. 10th Congreso de Exploración y Desarrollo de Hidrocarburos, Sesiones Generales: Energía y Sociedad, aliados inseparables, Instituto Argentino del Petróleo y el Gas, 877–890; https://www.researchgate.net/publication/328826691_AFLORAMIENTOS_TRIDIMENSIONALES_DE_PALEOCANALES_EXHUMADOS_GRUPO_CHUBUT_CUENCA_DE_CANADON_ASFALTO_COMO_ANALOGOS_DE_RESERVORIOS

Ghosh, S., Guchhait, S.K., 2019. Modes of formation, Palaeogene to Early Quaternary palaeogenesis and geochronology of laterites in Rajmahal Basalt Traps and Rarh Bengal of Lower Ganga Basin. Quaternary Geomorphology in India (eds. B.C. Das et al.): 25–60; https://doi.org/10.1007/978-3-319-90427-6_2

Giegengack, R.F., Zaki, A.S., 2017. Inverted topographic features, now submerged beneath the water of Lake Nasser, document a morphostratigraphic sequence of high-amplitude late Pleistocene climate oscillation in Egyptian Nubia. Journal of African Earth Sciences, **136**: 176–187; https://doi.org/10.1016/j.jafrearsci.2017.06.027

Girard, F., Ghienne, J.F., Rubino, J.L., 2012. Channelized sandstone bodies ('cordons') in the Tassili N'Ajjer (Algeria & Libya): snapshots of a Late Ordovician proglacial outwash plain. Geological Society Special Publications, **368**: 355–379; https://doi.org/10.1144/SP368.3

Grabowska-Olszewska, B., 2004. The behavior of cohesive soils in the flood and draught condition (in Polish with English summary). Inżynieria Środowiska, **12**, Zeszyty Naukowe, **131**: 107–112.

Gumbricht, T., McCarthy, J., McCarthy, T.S., 2004. Channels, wetlands and islands in the Okavango Delta, Botswana, and their relation to hydrological and sedimentological processes. Earth Surface Processes and Landforms, **29**: 15–29; https://doi.org/10.1002/esp.1008

Harasimiuk, M., 1975. Relief evolution of the Chełm Hills in the Tertiary and Quaternary (in Polish with English summary). Prace Geograficzne, **115**.

Harasimiuk, M., Henkiel, A., 1980a. Objaśnienia do Szczegółowej Mapy Geologicznej Polski 1:50 000. Arkusz Łęczna (750) (in Polish). CAG, Warszawa; https://bazadata.pgi.gov.pl/data/smgp/arkusze_txt/old/smgp0750old.pdf

Harasimiuk, M., Henkiel, A., 1980b. Szczegółowa Mapa Geologiczna Polski 1:50 000, ark. Łęczna (750) (in Polish). CAG, Warszawa; https://bazadata.pgi.gov.pl/data/smgp/arkusze_skany/old/smgp0750old.jpg

Harasimiuk, M., Henkiel, A., 1981. Fossil valley forms in the vicinities of Łęczna and their importance for palaeoeography of the Wieprz River drainage system (in Polish with English summary). Geological Quarterly, **25** (1): 147–161.

Harasimiuk, M., Szwajgier, W., Terpiłowski, S., 2004. Wpływ lądolodu zlodowacenia Warty na rzeźbę północnego przedpola Wyżyny Lubelskiej (in Polish). In: Zlodowacenie Warty w Polsce (eds. M. Harasimiuk and S. Terpiłowski): 163–171. Wydaw. UMCS, Lublin.

Harasimiuk, M., Szwajgier, W., Jezierski, W., 2017. Szczegółowa Mapa Geologiczna Polski w skali 1:50 000. Arkusz Siedliszcze (751) (in Polish). CAG, Warszawa; https://bazadata.pgi.gov.pl/data/smgp/arkusze_skany/smgp0751.jpg

Hayden, A.T., Lamb, M.P., Fischer, W.W, Ewing, R.C., McElroy, B.J., Williams, R.M.E., 2019. Formation of sinuous ridges by inversion of river-channel belts in Utah, USA, with implications for Mars. Icarus, **332**: 92–110; https://lamb.caltech.edu/documents/19707/Hayden_et_al_2019.pdf

Hill, S.M., Eggleton, R.A., Taylor, G., 2003. Neotectonic disruption of silicified palaeovalley systems in an intraplate, cratonic landscape: Regolith and landscape evolution of the Mulculca range-front, Broken Hill Domain, New South Wales. Australian Journal of Earth Sciences, **50**: 691–707; https://www.tandfonline.com/doi/abs/10.1111/j.1440-0952.2003.01020.x

Hou, B., Fabris, A.J., Keeling, J.L., Fairclough, M.C., 2007. Cenozoic paleochennel-hosted uranium and current exploration methods, South Australia. MESA Journal, **46**: 34–39.

Hrynowiecka, A., Żarski, M., Drzewicki, W., 2019. The rank of climatic oscillations during MIS 11c (OHO and YHO) and postinterglacial cooling during MIS 11b and MIS 11a in eastern Poland. Geological Quarterly, **63** (2): 375–394; https://doi.org/10.7306/gq.1470

Jacobsen, R.E., Burr, D.M., 2017. Dichotomies in the fluvial and alluvial fan deposits of the Aeolis Dorsa, Mars: Implications for weathered sediment and paleoclimate. Geosphere, **13**: 2154–2168; https://doi.org/10.1130/GES01330.1

Janczyk-Kopikowa, Z., 1981. Pollen analysis of the Pleistocene sediments at Kaznów and Krępiec (in Polish with English summary). Biuletyn Instytutu Geologicznego, **321**: 249–258.

Keller, S.M., Morgan, M.L., 2016. Overview of the Eocene Castle Rock Conglomerate, eastcentral Colorado: Remapping the fluvial system, and implications for the history of the Colorado Piedmont and Front Range. GSA Field Guide, **44**: 125–141; https://doi.org/10.1130/2016.0044(05)

Kowalski, W.C., 1961. Wytrzymałość na ściskanie budowlanych skał senońskich przełomowego odcinka Wisły środkowej na tle ich litologii (in Polish). Biuletyn Geologiczny, **1**.

Krawczyk, M., 2023a. Objaśnienia do Szczegółowej Mapy Geologicznej Polski w skali 1:50 000. Arkusz Ostrów Lubelski (714) (in Polish). CAG, Warszawa; https://bazadata.pgi.gov.pl/data/smgp/arkusze_txt/smgp0714.pdf

Krawczyk, M., 2023b. Szczegółowa Mapa Geologiczna Polski w skali 1:50 000. Arkusz Ostrów Lubelski (714) (in Polish). CAG, Warszawa; https://bazadata.pgi.gov.pl/data/smgp/arkusze_skany/smgp0714.jpg

Krawczyk, M., Kamiński, M., 2024. Badania geofizyczne metodą tomografii elektrooporowej w rejonie Łęcznej na Polesiu. CAG, Warszawa nr inw. 2708/2024.

Krawczyk, M., Kucharska, M., 2023a. Objaśnienia do Szczegółowej Mapy Geologicznej Polski w skali 1:50 000. Arkusz Łęczna (750) (in Polish). CAG, Warszawa; https://bazadata.pgi.gov.pl/data/smgp/arkusze_txt/smgp0750.pdf

Krawczyk, M., Kucharska, M., 2023b. Szczegółowa Mapa Geologiczna Polski w skali 1:50 000. Arkusz Łęczna (750) (in Polish). CAG, Warszawa; https://bazadata.pgi.gov.pl/data/smgp/arkusze_skany/smgp0750.jpg

Krawczyk, M., Kucharska, M., 2024. Forms of sinuous ridges (inverted channels) in the Lublin region. An attempt to determine the genesis and reference to selected morphological forms occurring on Earth and Mars (in Polish). In: IV Polski Kongres Geologiczny, Poznań, Abstract book: 85; https://4pkg.amu.edu.pl/wp-content/uploads/2024/06/IVPKG_streszczenia.pdf

Kucharska, M., 2023a. Objaśnienia do Szczegółowej Mapy Geologicznej Polski w skali 1:50 000. Arkusz Orzechów Nowy (715) (in Polish). CAG, Warszawa; https://bazadata.pgi.gov.pl/data/smgp/arkusze_txt/smgp0715.pdf

Kucharska, M., 2023b. Szczegółowa Mapa Geologiczna Polski w skali 1:50 000. Arkusz Orzechów Nowy (715) (in Polish). CAG, Warszawa; https://bazadata.pgi.gov.pl/data/smgp/arkusze_skany/smgp0715.jpg

Kucharska, M., 2025a. Szczegółowa Mapa Geologiczna Polski w skali 1:50 000. Arkusz Sawin (752) (in Polish). CAG, Warszawa; https://bazadata.pgi.gov.pl/data/smgp/arkusze_txt/smgp0752.pdf

Kucharska, M., 2025b. Objaśnienia do Szczegółowej Mapy Geologicznej Polski w skali 1:50 000. Arkusz Sawin (752) (in Polish). CAG, Warszawa; https://bazadata.pgi.gov.pl/data/smgp/arkusze_skany/smgp0752.jpg

Kucharska, M., Krawczyk, M., 2023a. Objaśnienia do Szczegółowej Mapy Geologicznej Polski w skali 1:50 000. Arkusz Lubartów (713) (in Polish). CAG, Warszawa; https://bazadata.pgi.gov.pl/data/smgp/arkusze_txt/smgp0713.pdf

Kucharska, M., Krawczyk, M., 2023b. Szczegółowa Mapa Geologiczna Polski w skali 1:50 000. Arkusz Lubartów (713) (in Polish). CAG, Warszawa; https://bazadata.pgi.gov.pl/data/smgp/arkusze_skany/smgp0713.jpg

Kucharska, M., Krawczyk, M., Hrynowiecka, A., 2024. Evolution of the hydrographic network in the middle Wieprz River Basin (E Poland). Geological Quarterly, **68**, 15; https://doi.org/10.7306/gq.1743

LeConte, J., 1880. The old river beds of California. American Journal of Science, **19**: 176–190; https://doi.org/10.2475/ajs.s3-19.111.176

LeConte, J., 1886. A post-Tertiary elevation of the Sierra Nevada shown by the river beds. American Journal of Science, **32**: 167–181; https://doi.org/10.2475/ajs.s3-32.189.167

Lambeck, K., Yokoyama, Y., Purcell, T., 2002. Into and out of the Last Glacial Maximum: sea-level change during Oxygen Isotope Stages 3 and 2; Quaternary Science Reviews, **21**: 343–360; https://doi.org/10.1016/S0277-3791(01)00071-3

Lindner, L., Marks, L., 2008. Pleistocene stratigraphy of Poland and its correlation with stratotype sections in the Volhynian Upland (Ukraine). Geochronometria, **31**: 31–37; https://doi.10.2478/v10003-008-0014-9

Lisicki, S., 2003. Lithotypes and lithostratigraphy of tills of the Pleistocene in the Vistula drainage basin area, Poland (in Polish with English summary). Prace Państwowego Instytutu Geologicznego, **177**.

Liszkowski, J., 1979a. Objaśnienia do Szczegółowej Mapy Geologicznej Polski 1:50 000, ark. Ostrów Lubelski (714) (in Polish). CAG, Warszawa; https://bazadata.pgi.gov.pl/data/smgp/arkusze_txt/old/smgp0714old.pdf

Liszkowski, J., 1979b. Szczegółowa Mapa Geologiczna Polski 1:50 000, ark. Ostrów Lubelski (714) (in Polish). CAG, Warszawa; https://bazadata.pgi.gov.pl/data/smgp/arkusze_skany/old/smgp0714old.jpg

Luccihtta, I., Holm, F.R., Luccihtta, B.K., 2011. A Miocene river in northern Arizona and its implications for the Colorado River and Grand Canyon. GSA Today, **21**: 4–10; https://doi.org/10.1130/G119A.1

Maizels, J., 1990. Raised channels as indicators of palaeohydrologic change-a case study from Oman. Palaeogeography, Palaeoclimatology, Palaeoecology, **76**: 241–277; https://doi.org/10.1016/0031-0182(90)90115-N

Marchetti, D.W., Dohrenwend, J.C., Cerling, T.E., 2005. Geomorphology and rates of landscape change in the Fremont River drainage, northwestern Colorado Plateau. GSA Field Guide, **6**: 79–100; https://doi.org/10.1130/2005.fld006(04)

Marks, L., 2023. Quaternary stratigraphy of Poland – current status. Acta Geologica Polonica, **73**: 307–340; https://doi.org/10.24425/agp.2023.145614

Marks, L., Karabanov, A., Nitychoruk, J., Bahdasarau, M., Krzywicki, T., Majecka, A., Pochocka-Szwarc, K., Rychel, J., Woronko, B., Zbucki, Ł., Hradunova, A., Hrychanik, M., Mamchyk, S., Rylova, T., Nowacki, Ł., Pielach, M., 2018. Revised limit of the Saalian ice sheet in central Europe. Quaternary International, **478**: 59–74; https://doi.org/ 10.1016/j.quantit.2016.07.043

Maruszczak, H., 1974a. Środowisko przyrodnicze Lubelszczyzny w czasach prahistorycznych (in Polish). Dzieje Lubelszczyzny, **I**: 25–67.

Maruszczak, H., 1974b. Zagadnienie genezy i wieku przełomu Wieprza pod Łęczną (in Polish). In: Przewodnik 12. Ogólnopolskiego Zjazdu Polskiego Towarzystwa Geograficznego: 69–72.

Maruszczak H., 2001. Rozwój rzeźby wschodniej części wyżyn metakarpackich w okresie posarmackim (in Polish). Przegląd Geograficzny, **73**: 253–280; https://rcin.org.pl/Content/1027/PDF/Wa51_3627_r2001-t73-z3_Przeg-Geogr.pdf

Matsubara, Y., Howard, A.D., Burr, D.M., Williams, R.M.E., Dietrich, W.E., Moore, J.M., 2015. River meandering on Earth and Mars: A comparative study of Aeolis Dorsa meanders, Mars and possible terrestrial analogs of the Usuktuk River, AK, and the Quinn River, NV. Geomorphology, **240**: 102–120; https://doi.org/10.1016/j.geomorph.2014.08.031

Matter, A., Mahjoub, A., Neubert, E., Preusser, F., Schwalb, A., Szidat, S., Wulf, G., 2016. Reactivation of the Pleistocene trans-Arabian Wadi ad Dawasir fluvial system (Saudi Arabia) during the Holocene humid phase. Geomorphology, **270**: 88–101; https://doi.org/10.1016/j.geomorph.2016.07.013

McQueen, K.G., Gonzalez, O.R., Roach, I.C., Pillans, B.J., Dunlap, W.J., Smith, M.L., 2007. Landscape and regolith features related to Miocene leucitite lava flows, El Capitan northeast of Cobar, New South Wales. Australian Journal of Earth Sciences, **54**: 1–17; https://doi.org/10.1080/08120090600923311

Mohrig, D., Heller, P., Paola, C., Lyons, W.J., 2000. Interpreting avulsion processes from ancient alluvial sequences: the Guadalope-Matarranya system (northern Spain) and Wasatch Formation (western Colorado). GSA Bulletin, **112**: 1787–1803; https://doi.org/10.1130/0016-7606(2000)112<1787:IAPFAA>2.0.CO;2

Morgan, A.M., Howard, A.D., Hobley, D.E.J., Moore, J.M., Dietrich, W.E., Williams, R.M.E., Burr, D.M., Grant, J.A., Wilson, S.A., Matsubara, Y., 2014. Sedimentology and climatic environment of alluvial fans in the Martian Saheki crater and a comparison with terrestrial fans in the Atacama Desert. Icarus, **229**: 131–156; https://doi.org/10.1016/j.icarus.2013.11.007

Myślińska E., 1996. Leksykon gruntoznawstwa (in Polish). Państw. Inst. Geol., Warszawa.

Ollier, C.D., Sheth, H.C., 2008. The High Deccan duricrusts of India and their significance for the „laterite" issue. Journal of Earth System Science, **117**: 537–551; https://doi.org/10.1007/s12040-008-0051-9

Pain, C.F., Ollier, C.D., 1995. Inversion of relief – a component of landscape evolution. Geomorphology, **12**: 151–165; https://doi.org/10.1016/0169-555X(94)00084-5

Pain, C.F., Clarke, J.D.A., Thomas, M., 2007. Inversion of relief on Mars. Icarus, **190**: 478–491; https://doi.org/10.1016/j.icarus.2007.03.017

Pacanowski G., 2021. Dokumentacja badań geofizycznych wykonanych metodą tomografii elektrooporowej (ERT) w ramach tematu: aktualizacja Szczegółowej Mapy Geologicznej Polski w skali 1:50 000 (I etap – 160 arkuszy) – arkusz Łęczna, Ostrów Lubelski (in Polish). CAG, Warszawa nr inw. 13029/2023.

Pawłowska A., Tracz A., 1975. Dokumentacja badań geofizycznych dla opracowania Szczegółowej Mapy Geologicznej Polski, 1:50 000, arkusze Łęczna i Urszulin. CAG, Warszawa nr inw. 755735/1975.

Pinińska, J., Dziedzic A., 2006. Właściwości wytrzymałościowe i odkształceniowe skał. Część V, Region Lubelski. Katalog, **9** (in Polish). Wydz. Geol. UW. Warszawa. 1–97; https://bazadata.pgi.gov.pl/data/smgp/arkusze_txt/smgp0679.pdf

Pochocka-Szwarc, K., 2023. Objaśnienia do Szczegółowej Mapy Geologicznej Polski w skali 1:50 000. Arkusz Kołacze (716) (in Polish). CAG, Warszawa; https://bazadata.pgi.gov.pl/data/smgp/arkusze_txt/smgp0716.pdf

Schuster, M., Roquin, C., Duringer, P., Brunet, M., Caugy, M., Fontugne, M., Mackaye, H.T., Vignaud, P., Chienne, J.F., 2005. Holocene Lake Mega-Chad paleoshorelines from space. Quaternary Science Reviews, **24**: 1821–1827; https://doi.org/10.1016/j.quascirev.2005.02.001

Sias, S., 2002. Plio-Pleistocenic evolution of Rio Mannu di Mores valley (Logudoro, northern Sardinia). Geografia Fisica e Dinamica Quaternaria, **25**: 135–148; http://www.glaciologia.it/wp-content/uploads/FullText/full_text_25_2/06_GFDQ_25_2_Sias_135_148.pdf

Smith, D.M., Zalasiewicz, J.A., Williams, M., Wilkinson, I., Redding, M., Begg, C., 2010. Holocene drainage of the English Fenland: roddons and their environmental significance. Proceedings of the Geologists' Association **121**, 256–269; https://doi.org/10.1016/j.pgeola.2010.06.002

Stanford, J.D., Hemingway, R., Rohling, E.J., Challenor, P.G., Medina-Elizalde, M., Lester, A.J., 2010. Sea-level probability for the last deglaciation: a statistical analysis of far-field records. Global and Planetary Change, **79**: 193–203; https://doi.org/10.1016/j.gloplacha.2010.11.002

Stochlak, J., 1979a. Szczegółowa Mapa Geologiczna Polski 1:50 000, ark. Parczew (678) (in Polish). CAG, Warszawa; https://bazadata.pgi.gov.pl/data/smgp/arkusze_skany/old/smgp0678old.jpg

Stochlak, J., 1979b. Objaśnienia do Szczegółowa Mapa Geologiczna Polski 1:50 000, ark. Parczew (678) (in Polish). CAG, Warszawa; https://bazadata.pgi.gov.pl/data/smgp/arkusze_txt/old/smgp0678old.pdf

Świeca, A., 2000. Spatial variability of chemical denudation in the upland part of the Vistula and Bug interflueve. Kras i Speleologia, **10**: 84–104.

Wang, Z.T., Lai, Z.P., Qu, J.J., 2017. Inverted relief landforms in the Kumtagh Desert of northwestern China: A mechanism to estimate wind erosion rates. Geological Journal, **52**: 131–140; https://doi.org/10.1002/gj.2739

Wang, J., Bhattacharya, J., 2018. Plan-view paleochannel reconstruction of amalgamated meaner belts, Cretaceous Ferron Sandstone, Notom Delta, South-Centeral Utah, USA. Journal of Sedimentary Research, **88**: 58–74; https://doi.org/10.2110/jsr.2017.77

Whitney, J.D., 1865. Report of Progress and Synopsis of the Field Work From 1860 to 1864. Geological Survey of California, **1**.

Williams, R.M.E., Edgett, K.S,. 2005. Valleys in the Martian Rock Record. Lunar and Planetary Science, **36**, 1099; https://www.researchgate.net/publication/234235161_Valleys_in_the_Martian_Rock_Record

Williams, R.M.E., Chidsey Jr, T.C., Eby, D.E., 2007. Exhumed Paleochannels in Central Utah – analogs for raised curvilinear features on Mars. Utah Geological Association Publication, **36**: 220–235; https://archives.datapages.com/data/uga/data/079/079001/221_ugs790221.htm

Williams, R.M.E., Irwin III, R.P., Zimbelman, J.R., 2009. Evaluation of paleohydrologic models for terrestrial inverted channels: Implications for application to Martian sinuous ridges. Geomorphology, **107**: 300–315; https://doi.org/10.1016/j.geomorph.2008.12.015

Williams, R.M.E., Irwin III, R.P., Zimbelman, J.R., Chidsey Jr, T.C., Eby, D.E., 2011. Field guide to exhumed paleochannels near Green River, Utah: Terrestrial analogs for sinuous ridges on Mars. GSA Special Papers, **483**: 483–505; https://doi.org/10.1130/2011.2483(29)

Williams, R.M.E., Irwin, R.P. III, Burr, D.M., Harrison, T., McClelland, P., 2013. Variability in martian sinuous ridge form: Case study of Aeolis Serpens in the Aeolis Dorsa, Mars, and insight from the Mirackina paleoriver, South Australia. Icarus, **225**: 308–324; https://doi.org/10.1016/j.icarus.2013.03.016

Williams, R.M.E., Moersch, J.E., Fergason, R.L., 2018. Thermophysical Properties of Martian Fluvial Sinuous Ridges: Inferences on "Inverted Channel" Induration Agent. Earth and Space Science, **5**: 516–528; https://doi.org/10.1029/2018EA000402

Williams, R.M.E., Irwin, R.P., Dobrea, E.Z.N., Howard, A.D., Dietrich, W.E., Cawley, J.C., 2021. Inverted channel variations identified on a distal portion of a bajada in the Central Atacama Desert, Chile. Geomorphology, **393**, 107925; https://doi.org/10.1016/j.geomorph.2021.107925

Worden, R.H., Burley, S.D., 2003. Sandstone diagenesis: From sand to stone. IAS Reprint Series, **4**: 3–44; https://doi.org/10.1002/9781444304459.ch

Zaki, A.S., Giegengack, R., 2016. Inverted topography in the southeastern part of the Western Desert of Egypt. Journal of African Earth Sciences, **121**: 56–61; https://doi.org/10.1016/j.jafrearsci.2016.05.020

Zaki, A.S., Pain, C., Edgett, K.E., Giegengack, R., 2018. Inverted stream channels in the Western Desert of Egypt: synergistic remote, field observations and laboratory analysis on Earth with application to Mars. Icarus, **309**: 105–124; https://doi.org/10.1016/j.icarus.2018.03.001

Zaki, A.S., Giegengack, R., Castelltort, S., 2020. Inverted channels in the Eastern Sahara distribution, formation, and interpretation to enable reconstruction of paleodrainage networks, In: J. Herget, A. Fontana (eds) Palaeohydrology. Geography of the Physical Environment. Springer, Cham: 117–134; https://doi.org/10.1007/978-3-030-23315-0_6

Zaki, A.S., Pain, C., Edgett, K.E., Castelltort, S., 2021. Global inventory of fluvial ridges on Earth and lessons applicable to Mars. Earth-Science Reviews, **216**, 103561; https://doi.org/10.1016/j.earscirev.2021.103561

Zaki, A.S., Davis, J., Edgett, K., Giegengack, R., Roigé, M., Conway, S., Schuster, M., Gupta, S., Salese, F., Sangwan, K., Fairén, A., Hughes, C., Pain, C., Castelltort, S., 2022. Fluvial depositional systems of the African Humid Period: an analog for an early, wet Mars in the Eastern Sahara. Environmental Science, Geology Journal of Geophysical Research: Planets, **127**, e2021JE007087; https://ddd.uab.cat/pub/artpub/2022/292673/292673.pdf

Zieliński, T., 1995. Kod litofacjalny i litogenetyczny – konstrukcja i zastosowanie (in Polish). In: Badania osadów czwartorzędowych (eds. E. Mycielska-Dowgiałło and J. Rutkowski): 220–235. Uniwersytet Warszawski, Warszawa.

Zieliński, T., Pisarska-Jamroży M., 2012. Which features of deposits should be included in a code and which not? (in Polish with English summary). Przegląd Geologiczny, **60:** 387–397; https://www.pgi.gov.pl/en/docman-tree-all/publikacje-2/przeglad-geologiczny/2012-1/lipiec-2/1055-jakie-cechy-litologiczne/file.html

Żarski, M., 2023. Objaśnienia do Szczegółowej Mapy Geologicznej Polski w skali 1:50 000. Arkusz Parczew (678) (in Polish). CAG, Warszawa; https://bazadata.pgi.gov.pl/data/smgp/arkusze_txt/smgp0678.pdf

Żarski, M., Kucharska, M., 2020. Objaśnienia do Mapy geologicznej Polski w skali 1: 200 000, arkusz Siedlce (in Polish). CAG, Warszawa; https://bazadata.pgi.gov.pl/data/mgp200/txt/edycja2/mgp200txt41-edycja2.pdf

Żarski, M., Tekielska, A., 2023. Szczegółowa Mapa Geologiczna Polski w skali 1:50 000. Arkusz Parczew (678) (in Polish). CAG, Warszawa; https://bazadata.pgi.gov.pl/data/smgp/arkusze_skany/smgp0678.jpg

Żarski, M., Hrynowiecka, A, Górecki, A., Winter, H., Pochocka-Szwarc, K., 2024. The maximum extent of the Odranian Glaciation (Saalian, MIS 6) in the South Podlasie Lowland (SE Poland) in the light of sites with lacustrine deposits of the Mazovian Interglacial. Acta Geologica Polonica, **74**, 14; https://doi.org/10.24425/agp.2024.150006